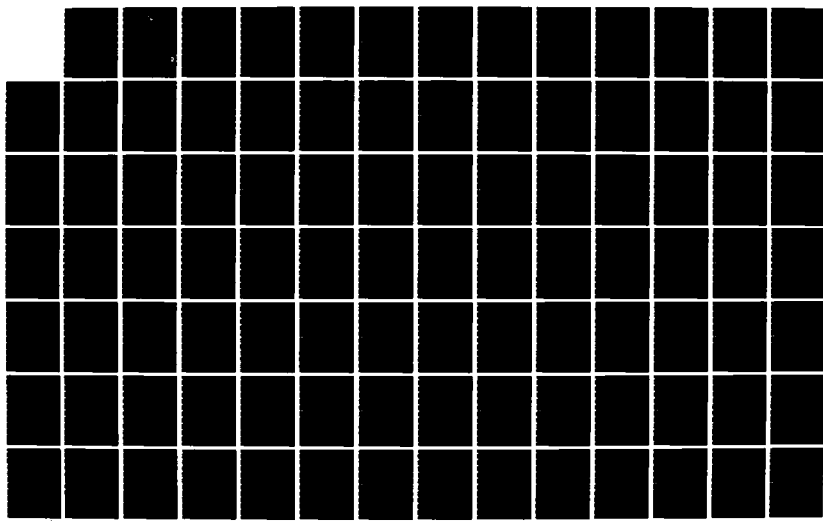
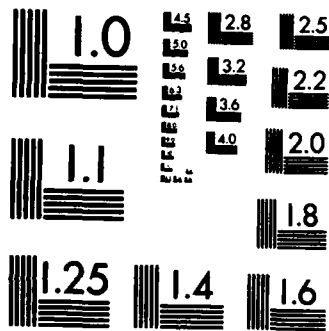


AD-A136 928 NONLINEAR MODELING AND INITIAL CONDITION ESTIMATION FOR 1/2  
IDENTIFYING THE A. (U) AIR FORCE INST OF TECH  
WRIGHT-PATTERSON AFB OH SCHOOL OF ENGI. C D LUTES  
UNCLASSIFIED DEC 83 AFIT/GRE/RA/83D-14 F/G 20/13 NL





MICROCOPY RESOLUTION TEST CHART  
NATIONAL BUREAU OF STANDARDS-1963-A

DTIC FILE COPY

AD A 136928



NONLINEAR MODELING AND INITIAL CONDITION  
ESTIMATION FOR IDENTIFYING THE AERO-  
THERMODYNAMIC ENVIRONMENT OF THE SPACE  
SHUTTLE ORBITER

THESIS

Charles D. Lutes  
Second Lieutenant, USAF  
AFIT/GAE/AA/83D-14

DTIC  
ELECTE  
S JAN 17 1984 D  
E

DEPARTMENT OF THE AIR FORCE  
AIR UNIVERSITY

**AIR FORCE INSTITUTE OF TECHNOLOGY**

Wright-Patterson Air Force Base, Ohio

84 01 17 074

This document has been approved  
for public release; its  
distribution is unlimited.

①

NONLINEAR MODELING AND INITIAL CONDITION  
ESTIMATION FOR IDENTIFYING THE AERO-  
THERMODYNAMIC ENVIRONMENT OF THE SPACE  
SHUTTLE ORBITER

THESIS

Charles D. Lutes  
Second Lieutenant, USAF  
AFIT/GAE/AA/83D-14

DTIC

Approved for public release; distribution unlimited

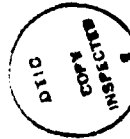
NONLINEAR MODELING AND INITIAL CONDITION ESTIMATION  
FOR IDENTIFYING THE REENTRY AEROTHERMODYNAMIC  
ENVIRONMENT OF THE SPACE SHUTTLE ORBITER

THESIS

Presented to the Faculty of the School of Engineering  
of the Air Force Institute of Technology  
Air University  
In Partial Fulfillment of the  
Requirements for the Degree of  
Master of Science in Aeronautical Engineering

Charles D. Lutes, B.S.E.  
Second Lieutenant, USAF

December 1983



Accession For	
NTIS GRA&I	<input type="checkbox"/>
DTIC TAB	<input type="checkbox"/>
Unannounced	<input type="checkbox"/>
Justification	
By _____	
Distribution/ _____	
Availability Codes _____	
Dist	Airline and/or Special
A-1	

Approved for public release; distribution unlimited

## Preface

Ever since the beginnings of manned flight, the science of flight test research has "suffered" from the glamorous image of the reckless, silken-scarfed test pilot careening through the sky in defiant contempt of fate. But in reality, actual flight tests are conducted with countless hours of exhaustive engineering analysis. As expectations and requirements for manned flying vehicles have increased exponentially over the years, so has the complexity of the problems faced by flight researchers. Today, some eighty years since Kitty Hawk, the Space Shuttle routinely delves into out space, far beyond the hopes and dreams of Orville and Wilbur Wright. The immense challenge of returning such a vehicle through an extreme, and virtually unknown, reentry environment has been conquered; thanks to the development of highly complex analysis tools, such as the HEATEST program described in this report. The true heroes, in this and all flight research efforts, are the engineers and pilots who have overcome each new engineering obstacle. To them, this report is dedicated, in the hopes that with each small contribution, a better understanding of ourselves and the world around us may be gained.

Many thanks are due to those who have aided in the

completion of this report. The personnel at the Air Force Flight Test Center at Edwards, AFB have provided much aid and support. My "mentors" at the Air Force Institute of Technology, particularly Major David R. Audley and Dr. Peter S. Maybeck, have provided much insight and concern throughout the investigation. Finally, my deepest gratitude is extended to Capt. James K. Hodge, for getting me through this effort in spite of myself.

Charles D. Lutes

## List of Figures

Figure	Page
1. System Identification of the Aerothermodynamic Environment of the Space Shuttle Orbiter .....	5
2. Space Shuttle Control Point Locations .....	10
3. A Cross-Section of the TPS Thermal Model .....	12
4. HEATEST Data Reduction Technique with Intial Condition Smoothing .....	35
C.1. Simulated Thermocouple Data (Two Segment Model) .....	75
C.2. Simulated Two Segment Heating Model .....	77
C.3. Simulated Thermocouple Data (Three Segment Model) .....	78
C.4. Simulated Three Segment Heating Model .....	80
D.1. Lower Surface STS-2 Flight Thermocouple Data (Mach 20 Pushover Pullup Maneuver) .....	82
D.2. STS-2 Lower Surface Heating Estimates .....	84
D.3. OMS Pod STS-2 Flight Thermocouple Data (Mach 20 Pushover Pullup Maneuver) .....	85
D.4. Time Segment Heating Estimates for OMS Pod STS-2 Data .....	87
D.5. Two Segment Model Heating Estimate for OMS Pod STS-2 Data .....	88
D.6. Three Segment Model Heating Estimate for OMS Pod STS-2 Data .....	89
D.7. Heating Estimates for Various Time Skews in OMS Pod STS-2 Data .....	91
D.8. Parameter Estimates for Various Time Skews in OMS Pod STS-2 Data .....	92
D.9. Average Error of Thermocouple Nodes for OMS Pod STS-2 Data .....	93

E.1.	Smoothing Simulation Thermocouple Data .....	95
E.2.	Initial Condition Smoothing for a Thermocouple Node Point (Node 5) .....	97
E.3.	Initial Condition Smoothing for a Non- Thermocouple Node Point (Node 3) .....	98
F.1.	STS-4 Lower Surface Thermocouple Data with Initial Condition Smoothing (Mach 12 POPU) .....	100
F.2.	Smoothed Initial Temperature Profile for STS-4 Lower Surface Plug .....	102
F.3.	Heating Estimates for STS-2/STS-4 Lower Surface .....	103

## List of Tables

Table	Page
C-1. Estimates for a Two Segment Model Simulation .....	76
C-2. Estimates for a Three Segment Model Simulation .....	79
D-1. Estimates for STS-2 Lower Surface .....	83
D-2. Estimates for STS-2 OMS Pod .....	86
D-3. Estimates for Various Time Skews in STS-2 OMS Pod Data .....	90
E-1. Smoothing Simulation Results .....	96
F-1. STS-4 Lower Surface Initial Condition Smoothing .....	101

### List of Symbols

A,B,C,D	Coefficient Matrices
$c_i$	Material Specific Heat
$E\{\cdot\}$	Stochastic Expectation
$f$	Probability Density Function
$f(\rho)$	Heating Rate Ratio ( $q/q_r$ )
H	Thermocouple Measurement Matrix
h	Enthalpy
I	Identity Matrix
J	Conditional Information Matrix
K	Kalman Gain Matrix
$k_i$	Material Thermal Conductivity
k	Total Number of Model Parameters
$L\{\cdot\}$	Likelihood Function
M	Mach Number
m	Total Number of Thermocouples
n	Total Number of Node Points
P	Covariance Matrix
Q	White Noise Strength Matrix
q	Heating Rate
$q_r$	Reference Heating Rate
$q_0$	Heating Ratio Intercept
$q(\cdot)$	Heating Derivative
R	Measurement Error Strength Matrix

$\bar{R}$	Spatial Correlation Matrix
RC	RC Time Constant
RE	Reynolds Number
$T_\infty$	Free Stream Temperature
t	Time
$\underline{u}$	Temperature State Vector
$u_\theta$	Parameter Sensitivity
v	Velocity
w	Model Noise Vector
Y	Measurement Time History
$\underline{y}$	Measurement Vector
$\alpha$	Angle of Attack
$\beta$	Sideslip Angle
$\delta$	Deflection Angle
$\epsilon$	Emissivity
$\Xi$	Parameter Vector
$\sigma$	Stefan-Boltzmann Constant
$\tau$	Spatial Error Matrix
$\mu$	Viscosity
$\underline{\mu}$	Measurement Noise Vector
$\rho$	Density
$\Phi_B$	Thermal Conductivity Factor
$\Phi\{\cdot\}$	State Transition Matrix
$\phi$	Noise Coefficient
$\Delta x_i$	Distance Between Node Points
$\Delta x_A$	Coating Thickness

Superscripts

+	A Posteriori Value
-	A Priori Value
^	State Estimate
*	Parameter Estimate
T	Transpose
-1	Inverse

Subscripts

i,j,k	Spatial or Temporal Description
0	Initial Condition
0	Reference Value
$\infty$	Free Stream Condition

### Abstract

This report describes improvements made to the data analysis tool HEATEST, used for identification of the reentry aerothermodynamic environment of the Space Shuttle Orbiter. The heating model was changed from a linear perturbation form to that of a piecewise linear interpolation form to account for nonlinear heating rates. Also, a fixed-point initial condition smoother was incorporated to gain better estimates of unknown initial temperatures. The development of both of these improvements is described, as well as the overall adaptive estimation process employed by the HEATEST scheme. Verification of these modifications was accomplished by applications to both simulated and actual flight test data.

Simulations of nonlinear heating rates indicated higher than actual coating thickness predictions for the linear perturbation model previously used. Flight results using the improved heating model provided additional verification of a time skew due to nonisothermal wall effects on the OMS pod. Estimation of initial temperatures using the fixed-point initial condition smoother enabled the identification of an unmodeled Mach or Reynolds number effect on the lower surface during the Mach 12 Pushover Pullup maneuver of STS-4.

## Table of Contents

	<u>Page</u>
Preface. . . . .	ii
List of Figures . . . . .	iv
List of Tables. . . . .	vi
List of Symbols . . . . .	vii
Abstract. . . . .	x
I. Introduction . . . . .	1
1.1 Background. . . . .	2
1.2 Objectives. . . . .	4
1.3 Overview. . . . .	7
II. Modeling the Aerothermodynamic Environment . . .	8
2.1 Modeling Assumptions. . . . .	8
2.2 Thermal Model . . . . .	11
2.3 Heating Model . . . . .	16
2.4 Stochastic Models . . . . .	19
2.5 Summary . . . . .	23
III. Identifying the Aerothermodynamic Environment . . . . .	24
3.1 Maximum Likelihood Criterion. . . . .	24
3.2 State Estimation. . . . .	27
3.3 Parameter Estimation. . . . .	30
3.4 Algorithm Summary . . . . .	34
IV. Initial Condition Smoothing . . . . .	37
4.1 Smoothing Techniques. . . . .	37
4.2 Fixed-Interval Smoothing. . . . .	39
4.3 Fixed-Point Smoothing . . . . .	42
4.4 Smoothing Algorithm . . . . .	44
4.5 Summary . . . . .	46
V. Results . . . . .	48
5.1 Approach. . . . .	48
5.2 Heating Model Simulation. . . . .	50
5.3 Heating Model Flight Data . . . . .	52

5.4	Simulation with initial Condition Estimation . . . . .	55
5.5	Flight Results with Initial Condition Estimation . . . . .	56
5.6	Summary . . . . .	57
VI.	Conclusions and Recommendations . . . . .	58
6.1	Conclusions . . . . .	58
6.2	Recommendations . . . . .	59
6.3	Summary . . . . .	61
	Bibliography . . . . .	63
	Appendix A: Piece-wise Linear Interpolation . . . . .	66
	Appendix B: Backwards Heat Equation . . . . .	71
	Appendix C: Heating Model Simulation Results . . . . .	74
	Appendix D: Heating Model Flight Data Results . . . . .	81
	Appendix E: Initial Condition Estimation Simulation Results . . . . .	94
	Appendix F: Initial Condition Estimation Flight Data Results . . . . .	100
	Vita . . . . .	104

## I. Introduction

### 1.1 Background

The Space Shuttle Transportation System (STS) has offered the engineering community a unique opportunity to flight test a reentry, hypersonic vehicle. The key to the Shuttle's versatility is its reusability, which is inherently dependent upon the Orbiter's ability to withstand a severe, and sometimes unknown, aerodynamic environment upon reentry. With this in mind, the National Aeronautics and Space Administration (NASA), in conjunction with the Air Force Flight Test Center (AFFTC), has initiated a flight test program designed to eliminate uncertainties about this environment and thus expand the operational capabilities of the system (Refs. 7,8,9,10). Although the initial test flights have now been completed, data analysis and expansion of the existing data base continues.

The ability to withstand this harsh reentry environment is provided by the Orbiter's Thermal Protection System (TPS). This system consists primarily of low density ceramic tiles, which insulate the underlying aluminum or graphite-epoxy structure. These tiles typically have highly radiative surfaces, offering additional protection from the heat transfer effects of aerodynamic

forced convection. The TPS consists of a variety of materials (Ref 1): Reusable Carbon-Carbon (RCC), used primarily on high temperature areas such as the nose cap and the wing leading edge; Flexible Reusable Surface Insulation (FRSI), a Nomex felt substance found on the upper surface where lower temperatures are expected; and two kinds of silicon based tiles, High/Low temperature Reusable Surface Insulation (HRSI/LRSI), used on the lower surface and other high heat load areas where RCC is not needed.

The capabilities of the TPS directly affect the performance of the reentry Orbiter and its ability to perform a specified mission. For this reason, the Orbiter Flight Test program (OFT) developed by NASA and AFFTC has included flight test techniques designed to assess the TPS capabilities and identify the reentry aerothermodynamic environment (Ref 10).

Initial phases of the OFT consisted of real time engineering simulation of the reentry process. Suitable simulation models were needed to estimate the aerothermodynamic envelope for safe mission planning of the initial test flights and for subsequent analysis of the flight test data. These models, developed by AFFTC, are described in Chapter II of this paper. Unknown parameters were originally estimated by theoretical considerations and ground testing.

Flight test maneuvers required adequate data acquisition processes. For assessing aerothermodynamic capabilities, temperature variations are considered crucial. During the flight test phase, instrumentation consisting of temperature-sensing thermocouples provided this information. Surface thermocouples were imbedded under a thin coating of the RSI tiles on several locations on the Orbiter.

Simulation of thermocouple response indicated that transients in vehicle attitude (angle of attack, sideslip, and control surface deflection) were important, in addition to trajectory and atmosphere. Transient flight test maneuvers were developed by AFFTC (Ref 10) and incorporated into the flight test program. These maneuvers, such as the Pushover Pullup (POPU) maneuver, were designed to provide transients in vehicle attitude for durations long enough for thermocouple response but short enough to avoid affecting the reentry profile.

The final phase of the program consists of data reduction and analysis designed to identify the aerothermodynamic environment and update the models of the engineering simulation for subsequent envelope expansion. A method of analysis was designed by AFFTC in the form of a digital computer program called HEATEST (HEATing ESTimation) (Refs 1,7,8,9,10).

The HEATEST algorithm is based on system identification theory (Ref 5). The simulator models, applied in a stochastic context, are combined with thermocouple measurements in a state/temperature estimation (Kalman filter) routine. Best estimates of the unknown model parameters are made using parameter estimation techniques (Refs 2,5,15). The combined state and parameter identification technique provides best estimates for both temperatures and aerothermodynamic model parameters.

Figure 1 (Ref 1), provides a summary of the system identification process used to identify the aerothermodynamic environment of the Space Shuttle Orbiter.

### 1.2 Objectives

Although the HEATEST program has worked well in the analysis process, several areas for improvement have been identified (Refs 1,7,8,9,10,11). The purpose of this investigation is to analyze these areas, make improvements in the estimation scheme, and to incorporate them into the HEATEST program.

One aspect in which the estimation process has had difficulties is in properly identifying areas with severe nonlinearities. Because the original models were based on a linear perturbation form, nonlinear heating rates resulting from geometric discontinuities, flow irregularities, and other unmodelled effects have been difficult to

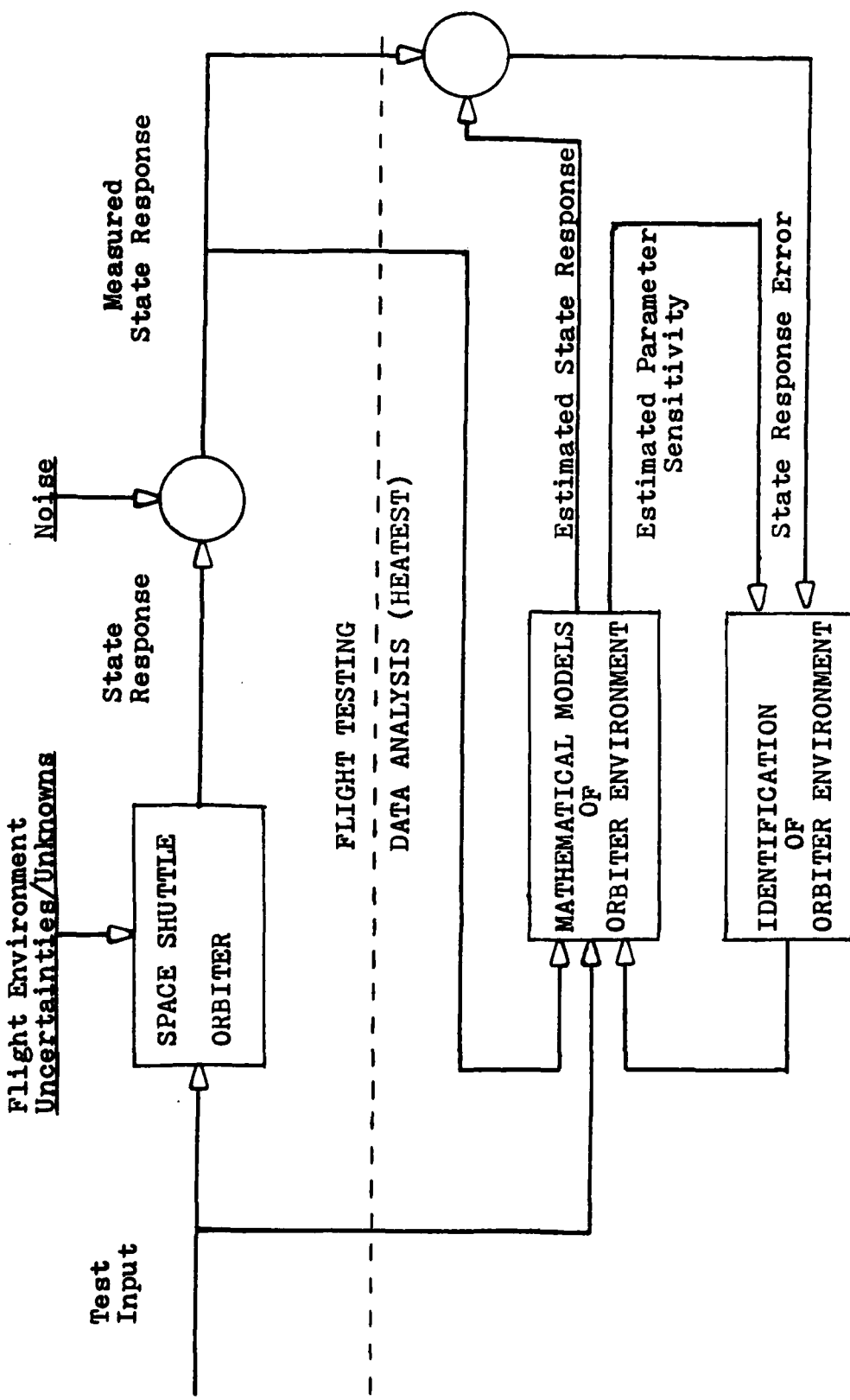


Figure 1. System Identification of the Aerothermodynamic Environment of the Space Shuttle Orbiter

estimate. Attempts to handle these nonlinearities have included the processing of maneuver data in small time segments and then correlating the results (Ref 9). Difficulties in correlation, convergence problems, and excessive computer time make these methods undesirable in some cases. Thus one objective of this investigation is to enhance the aerothermodynamic models to account for these nonlinearities directly. The method developed by this report assumes a piecewise linear heating rate, providing the models with the required flexibility.

Inaccurate initial conditions used for initializing the estimation process have provided questionable results in some cases (Ref 8). Generation of these initial conditions is a difficult process, and one method of improvement is to estimate these conditions based on the maneuver data (Ref 1). The development and incorporation of a fixed-point initial condition "smoother" is another aspect of this paper.

Testing and application of the modified program is necessary for verification of the validity of the improvements. Simulated data, for which the results are known, are processed for testing purposes. Application to real flight data where problems have occurred previously will complete the testing phase and provide additional insight into the results of the flight test program.

### 1.3 Overview

Because the existing identification process is important to the overall understanding of the proposed modifications, details of the theoretical development of the estimation scheme are provided with emphasis on these modifications. The enhanced models, formulated from the original simulator models, are developed in Chapter II and Appendix A, and then placed in the stochastic setting needed for the identification effort. Chapter III highlights the estimation process, including the development of the maximum likelihood criterion on which the scheme is based. The initial condition smoother is developed in Chapter IV, with an associated discussion in Appendix B relating the difficulties of solving the model heat equation in a smoothing context. Testing and application results for both simulated and flight test data is given in Chapter V and Appendices C-F. Finally, conclusions about the validity of the modifications; discussion of important physical results from flight test data; and suggestions for further improvements are included in Chapter 6.

## II. Modeling The Aerothermodynamic Environment

### 2.1 Modeling Assumptions

Model equations for the reentry aerothermodynamic environment were originally developed for the AFFTC simulator and subsequently applied to the data reduction scheme HEATEST with some modifications. In developing these process models, a natural distinction was made between the diffusion equation model of heat transfer in the TPS (thermal model) and the surface boundary condition for aerodynamic forced convection and radiation (heating model) (Ref 1). The surface heating rate due to aerodynamic forced convection is a primary unknown and is described by the unknown parameters of the heating model. Observations of these unknowns occur in the thermal model i.e. the diffusive heat transfer behavior of the TPS material measured by thermocouple sensed temperature variations. Thus, adequate simulation or estimation of the aerothermodynamic environment must include both of these models.

The development of these models includes several assumptions. First, it is assumed that the thermal characteristics of the TPS materials (thermal conductivity,  $k$ ; specific heat capacity,  $c$ ; and density,  $\rho$ ) are known through laboratory tests and theoretical consideration. However, the thermal conductivity may be scaled by an

unknown thermal conductivity factor to account for pressure changes within the tile. Another assumption is that each Orbiter location is associated with a unique set of models. Thus the initial investigation has concentrated on seven control points (Figure 2) identified by NASA and AFFTC as critical to reentry trajectory shaping (Ref 1).

One assumption that has proven restrictive in some cases is that of an isothermal wall (Ref 11). The assumption is that the Orbiter wall, protected by the TPS, remains at a constant temperature and serves as a boundary condition for the thermal model. Subsequent analysis (Ref 11) has indicated that a jump in the wall temperature may occur at the interface of two dissimilar materials, thus producing a nonisothermal wall effect. Such an effect may significantly raise or lower heating from laminar predictions depending on the direction of the temperature jump. In the data reduction scheme described in this paper, the nonisothermal wall effect may take the form of increased/decreased heating or time skews caused by thermocouple lag during the transient maneuvers.

Finally, a major simplification is the assumption of a one-dimensional diffusion model for the heat transfer through the TPS (Ref 1). Although motivated primarily by computational tractability, this assumption proves to be

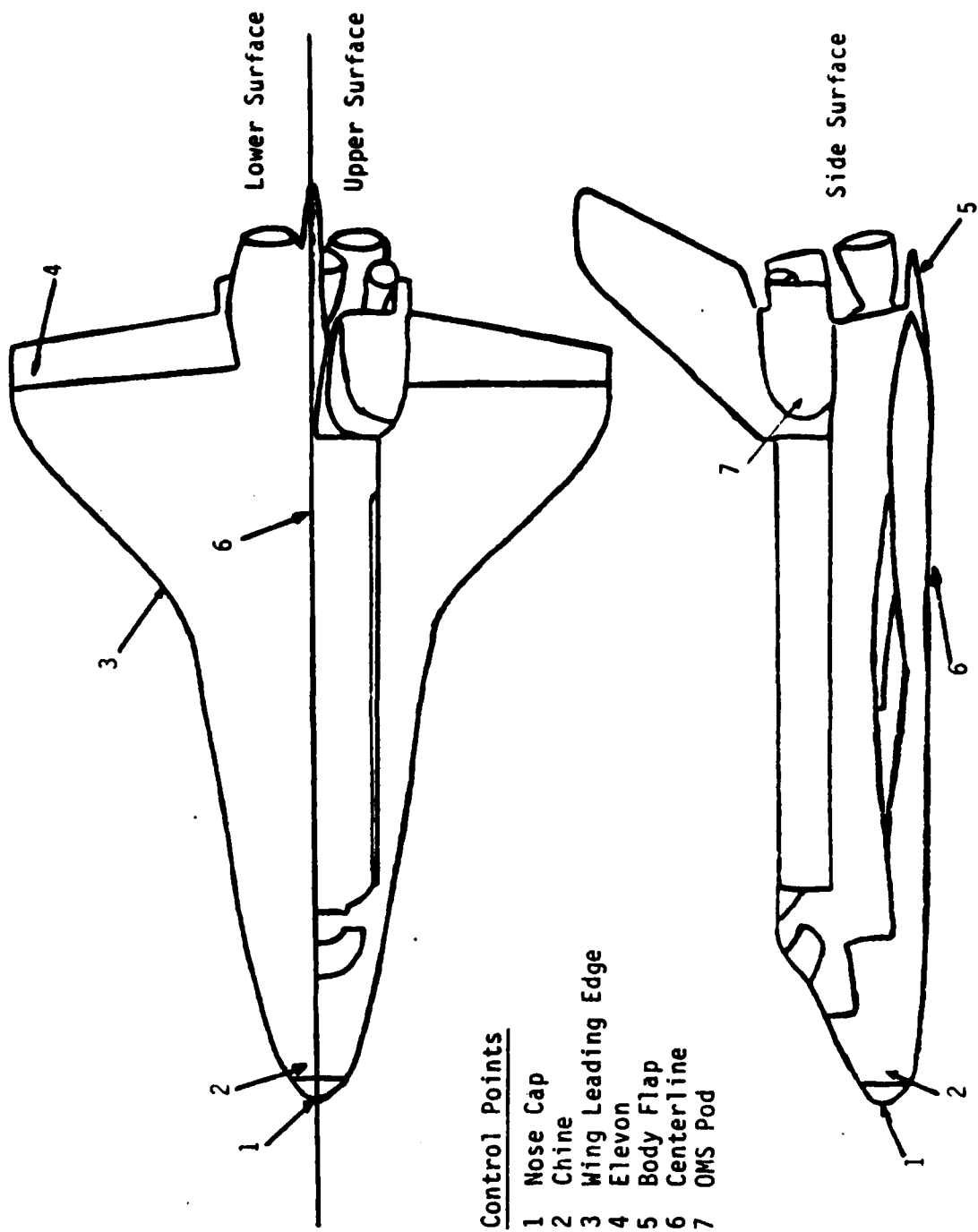


Figure 2. Space Shuttle Control Point Locations

an adequate description of what is largely a one-dimensional phenomena. Because of the low conductivity of the TPS material, the spanwise temperature gradients are assumed to be too small to affect the behavior of the temperature profile significantly for the short period of reentry. This model is developed more fully in the next section.

## 2.2 Thermal Model

A cross-section of the one-dimensional thermal model is given in Figure 3 as a typical Reusable-Surface-Insulation (RSI) tile. For implementation on a digital computer, n discrete node points were established to approximate the temperature profile throughout the tile. A surface thermocouple is normally located just under the surface coating (block A) at the second node point (i-2). Additional thermocouples may be embedded in the tile and node points are spaced so as to correspond with the embedded thermocouples. Blocks A through D represent different materials with thermal properties that vary with local temperature and pressure. A surface coating (block A) that is hand applied before flight, is modeled with an unknown thickness ( $\Delta X_A$ ). Block B represents the bulk of the TPS Material, and in general is assumed to have an unknown thermal conductivity factory,  $\phi_B$ . In block C, the RSI is bonded by Room-Temperature-Vulcanizing (RTV) adhesive to a nomex felt Strain-Isolation Pad (SIP), which in turn is bonded

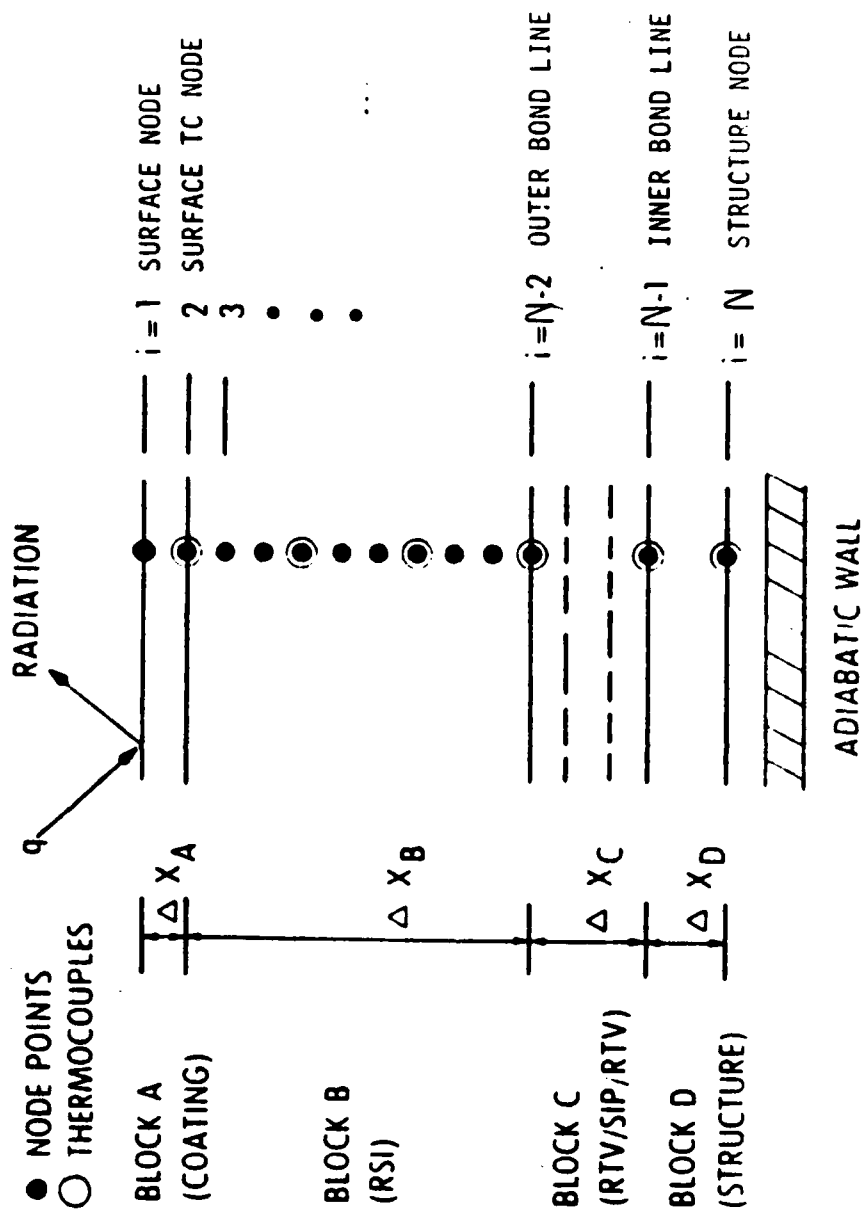


Figure 3. A Cross-Section of the TPS Thermal Model

to the structure by RTV. In block D, the effective structural thickness and heat sink complete the one-dimensional model where an adiabatic wall is assumed.

The convective heat rate ( $q$ ), obtained from the heating model, is applied to the surface node ( $i-1$ ) by the mechanism of forced aerodynamic convection. The surface, with a high emissivity, radiates most of the heat away but conducts a small amount into the TPS through the surface coating. The heat then diffuses throughout the TPS, causing variations in the temperature profile. An energy balance at each node point yields a system of  $n$  nonlinear differential equations of the form (Ref 8):

$$\begin{aligned} & \frac{(c_i \rho_i \Delta X_i + c_{i-1} \rho_{i-1} \Delta X_{i-1})/2}{U_i} = k_{i-\frac{1}{2}}/\Delta X_{i-1} U_{i-1} - \\ & (k_{i-\frac{1}{2}}/\Delta X_{i-1} + k_{i+\frac{1}{2}}/\Delta X_i) U_i + k_{i+\frac{1}{2}}/\Delta X_i U_{i+1} - \\ & \sigma \epsilon_i (U_i^4 - U_{i-1}^4) - \sigma \epsilon_{i+} (U_i^4 - U_{i+1}^4) + q_i \end{aligned} \quad (2-1)$$

where  $\epsilon_i$  is the radiative emissivity;  $\sigma$  is the Stefan-Boltzmann constant;  $c$  is the material specific heat;  $\rho$  is the material density; and  $k$  is the material conductivity. Additionally, the thermal conductivity of Block B,  $k_B$ , may be scaled by the thermal conductivity factor,  $\phi_B$ . Equation (2-1) includes terms describing the thermal conduction from adjacent node points ( $k_{i-\frac{1}{2}}/\Delta X_{i-1}$ ); surface radiation ( $\sigma \epsilon_i U_i^4$ ); and the heat rate due to aerodynamic

forced convection as obtained from the heating model ( $q_i$ ). Coefficients with subscripts which are less than one or greater than  $n$  are zero. The radiation and heat rate terms are zero except at the surface and backface nodes. The radiation sink temperature ( $U_o$  and  $U_{n+1}$ ) must be specified at the surface and backface nodes. The emissivities at the plus or minus side of the element ( $\epsilon_{i+}$  and  $\epsilon_{i-}$ ) are also zero except at the surface and backface nodes where they are assumed constant.

The solution of the system of equations (2-1) is needed for simulation and for the parameter estimation scheme described in Chapter III. These equations can be solved numerically from a given initial condition by approximating the time derivative. To insure stability with a minimum of numerical complexity, a first order backward difference form was chosen for the original simulator (Refs 8,9,10):

$$\dot{U}_i = (U_i(t_n) - U_i(t_{n-1})) / \Delta t \quad (2-2)$$

where  $\Delta t$  is the time step. The resulting system of implicit difference equations must be solved simultaneously. The surface node equation with the highly nonlinear radiation term was solved with a Newton-Raphson iteration and extrapolation scheme (Ref 24). A tridiagonal algorithm was used for the simultaneous solution of the remaining difference equations (Ref 8,9,10).

Numerical solution of (2-1) has resulted in an accurate simulation of surface and bondline temperatures at specific locations critical for mission evaluation (Ref 9). During initial testing and simulations, spatial and time steps sizes were varied to investigate accuracy (Ref 9). A spatial step of .00833 feet and time steps of up to one second yielded acceptable results (Ref 8). For the purpose of flight data reduction, this numerical scheme provides an adequate simulation of the temperature profile during transient maneuvers necessary for estimating the aerothermodynamic environment.

The environment to be identified thus consists of unknown parameters given in Equation (2-1). The value of the radiative emissivity,  $\epsilon$ , although thought to be approximatley .85, may degrade over the period of flight time and is known to vary with surface location and temperature. Thus, because of its importance in the surface boundary condition, it is desirable to estimate this parameter. Unfortunately, difficulties in estimating this parameter in many cases cause the nominal value to be used (Ref 10). The thickness of the surface coating,  $\Delta x_A$ , may vary significantly from its specified value of 15 mils due to the imprecise manner in which it is applied and is thus treated as unknown. The thermal conductivity factor,  $\phi_B$ , although generally assumed to have a value of unity, may

vary with local tile pressure and thus can be considered a candidate for estimation. Finally, the parameters that determine the heating rate ( $q$ ) as described in the next section, are estimated.

### 2.3 Heating Model

Heating models for several specific points on the Orbiter have been developed for the AFFTC simulator and the HEATEST program (Refs 1,8,9,10) to determine the heating rate ( $q$ ) in equation (2-1). Because of low material conductivity, it is assumed that this heating rate is, however, dependent upon changes in the vehicle attitude, trajectory, and atmosphere.

Nondimensionalizing by a reference heating rate,  $q_r$ , partially accounts for the heating rate dependence on the trajectory and atmosphere. The NASA method of calculating a reference heating rate for a one foot radius sphere was used as follows (Ref 20):

$$q_r = 17700 \sqrt{\rho_\infty} (V_\infty/10^4)^{3.07} (1-h_w/h_o) \quad (2-3a)$$

$$h_w = .24 (q_r/(\sigma\epsilon))^{.25} \quad (\text{wall enthalpy}) \quad (2-3b)$$

$$h_o = .24 T_\infty + V_\infty^2/50063 \quad (\text{stagnation enthalpy}) \quad (2-3c)$$

where the characterizing free stream variables are density ( $\rho_\infty$ ), velocity ( $V_\infty$ ), and temperature ( $T_\infty$ ). Alternative reference methods to account for other effects have also been established (Ref 8).

The dependence of the heating rate on parameters other than those included in the reference heating rate are summarized by the static transfer relation or heating ratio,  $f(\rho)$ . These parameters include body location (ie. there is a unique  $f(\rho)$  associated with each control point); angle of attack ( $\alpha$ ); sideslip ( $\beta$ ); control surface deflection ( $\delta_e$ , elevon;  $\delta_{bf}$ , bodyflap); Reynolds number (RE); and free stream Mach number ( $M_\infty$ ). Typically, the heating ratio has been cast in linear perturbation form (Ref 7):

$$f(\rho) = q/q_r = q_0 + q_\alpha(\alpha - \alpha_0) + q_\beta(\beta - \beta_0) + q_{RE}(RE - RE_0) \\ + q_{\delta_e}(\delta_e - \delta_{eo}) + q_{\delta_{bf}}(\delta_{bf} - \delta_{bf_0}) + q_{M_\infty}(M_\infty - M_\infty_0) \quad (2-4)$$

where  $q_0$  is the magnitude of the heating rate,  $q$ , at the reference conditions specified by the zero subscript on each variable. The subscripts on the heating rate indicate partial differentiation or slopes with respect to each variable. These "heating derivatives" are assumed to be locally constant for short time durations, similar to aerodynamic derivatives used in stability

theory. The heating derivatives are generally unknown and are appropriate for parameter identification.

In the presence of geometric nonlinearities, flow irregularities, and other unmodeled effects, the heating ratio may not be adequately described by a locally linear function of the form given in (2-4). To account for nonlinearities in the heating ratio, a new model has been developed. This model, derived from Lagrange interpolation theory (Ref 3,18), assumes a heating ratio that is piecewise linear with respect to the variable of concern (angle of attack for the case shown):

$$\begin{aligned} q_o + q_{\alpha 1}(\alpha - \alpha_o) + f(\beta, RE, \delta, M) & \quad \alpha < \alpha_1 \\ q_o + q_{\alpha 1}(\alpha_1 - \alpha_o) + q_{\alpha 2}(\alpha - \alpha_1) + f(\beta, RE, \delta, M) & \quad \alpha_1 < \alpha < \alpha_2 \\ f(\rho) = & \cdot \\ & \cdot \\ & \cdot \\ q_o + q_{\alpha 1}(\alpha_1 - \alpha_o) + \dots + q_{\alpha n}(\alpha - \alpha_n) + f(\beta, RE, \delta, M) & \quad \alpha < \alpha_{n-1} \end{aligned} \tag{2-5}$$

where the derivatives,  $q_1, q_2, q_n$ , and the break points,  $\alpha_1, \alpha_2, \dots, \alpha_n$ , are assumed constant for the maneuver

duration.

A more detailed description and development is given

in Appendix A. Also presented are model sensitivity equations needed for the estimation process of Chapter III. Typically, the derivatives,  $q_{\alpha_i}$ , and the break points or "knots",  $\alpha_i$ , are unknown and should be estimated. However, as discussed in the Appendix, difficulties may occur in estimating the locations of these break points and it may be necessary to specify them directly. For flight maneuvers with relatively small angle of attack sweeps, this approximation may not prove restrictive.

With the heating model thus described, a vector of unknown parameters may be defined for use in the system identification scheme of Chapter III. These include the radiative emissivity,  $\epsilon$ ; the surface coating,  $\Delta X_A$ ; the thermal conductivity factor,  $\Phi_B$ ; and the heating model derivatives contained in  $f(\rho)$ . This parameter vector,  $\Xi$ , is given by

$$\Xi = (\epsilon, \Delta X_A, \Phi_B, q_o, q_{\alpha_1}, \dots, q_{\alpha_n}, \alpha_1, \alpha_2, \dots, \alpha_n,$$

$$q_\beta, q_{\delta_e}, q_{\delta_{bf}}, q_{RE}, q_{M^\infty})$$

#### 2.4 Stochastic Models

The heating and thermal models presented thus far are complete for use in aerothermodynamic simulation. However, for accurate identification of the aerothermodynamic

environment, stochastic processes must be introduced to account for uncertainties in the modeling process, estimation scheme, and measurement methods. The resulting stochastic models are established in linear state space form and are amenable to state and parameter estimation.

Initial conditions for the temperature vector,  $\underline{u}(t)$ , are given by the stochastic equation

$$\underline{u}(t_0) = \underline{u}_0 + \underline{\gamma}_0 \quad (2-5)$$

where  $\underline{u}_0$  is the initial state vector; and the initial error ( $\underline{\gamma}_0$ ) is assumed to be a zero mean Gaussian process with an initial covariance matrix given by (Ref 8)

$$P_{ij} = \phi_{IC}^2 u_i(t_0) u_j(t_0) \bar{R}_{ij} \quad (2-6)$$

where  $\phi_{IC}$  represents the normalized deviation in initial temperatures and  $\bar{R}_{ij}$  defines the spatial correlation between node points. The error model for the stochastic process ( $\gamma$ ) is assumed to be stationary and spatially distributed with zero mean and covariance given by (Ref 8)

$$\bar{R}_{ij} = \exp\left(-\sum_{l=i}^j RC_l / \phi_{TR}\right) \quad (2-7a)$$

$$RC_l = \rho_l C_l \Delta X_l^2 / K_l \quad (2-7b)$$

where the subscripts i and j refer to the thermal nodes.

The constants  $\rho_\ell, c_\ell, K_\ell$ , and  $\Delta X_\ell$  are as defined previously for equation (2-1).  $RC_\ell$  is a thermal conduction time constant, analogous to that of electrical circuit theory, and represents an approximation to the amount of time (in seconds) that it takes a heat pulse to affect a given node point. The time constant is nondimensionalized by a characteristic time,  $\phi_{TR}$ , which represents a scaling factor for spatial correlation.

For the state estimation scheme described in Chapter III, a linear form of the diffusion model is needed, specifically for covariance propagation. By quasi-linearizing the nonlinear boundary term of (2-1) (Ref 9), a linear state space description of the temperature profile may be given as

$$\dot{\underline{u}}(t) = A \underline{u}(t) + \underline{B} + \underline{W}(t) \quad (2-8)$$

where  $\underline{u}(t)$  is the n-dimensional state vector representing the temperature profile at time t; A is an  $n \times n$  tridiagonal matrix of material properties; and  $\underline{B}$  is an n-dimensional vector containing the heating rate parameters and the quasi-linearized radiation terms of Equation (2-1).  $\underline{W}(t)$  is a n-dimensional, white stationary Gaussian process with statistics given by (Ref 1).

$$E\{\underline{W}(t)\} = \underline{0}$$

$$E\{\underline{W}(t) \underline{W}(t')\} = Q(t)\delta(t-t') \quad (2-9a)$$

where  $\delta(\cdot)$  is the delta function and the strength term is given by (Ref 9).

$$Q_{ij} = \begin{cases} (\phi_{ME}^2 + \phi_{BN}^2) \bar{R}_{ij} U_{eq}^2 & i=j=1 \\ \phi_{ME} \phi_{BN}^2 + \phi_{BN}^2 \bar{R}_{ij} U_{eq}^2 & i=1, j \neq 1 \\ \phi_{ME}^2 \bar{R}_{ij} U_{eq}^2 & i \neq 1, j \neq 1 \end{cases} \quad (2-9b)$$

The constant  $\phi_{BN}$  is the normalized deviation of the heating rate at the boundary and  $\phi_{ME}$  is the normalized deviation in the heat flux due to model error.  $U_{eq}$  is an equilibrium temperature calculated from  $q$  assuming no conduction.

Measurements made by thermocouples embedded in the TPS can be described by

$$\underline{y}(t_n) = H \underline{U}(t_n) + \underline{\mu}_n \quad (2-10)$$

where  $\underline{y}$  is an  $m$ -dimensional vector of thermocouple measurements and  $H$  is an  $m \times n$  matrix defined by

$$H_{ij} = \begin{cases} 1 & \text{if } u_j \text{ corresponds to } y_i \\ 0 & \text{if } u_j \text{ does not appear in } y_i \end{cases} \quad (2-11)$$

The error term  $\underline{\mu}_n$  includes thermocouple noise and instrumentation errors, especially quantization problems associated with an 8-bit data word length. All thermocouples are independent of each other and the model processes (Ref 1). The error term is thus assumed to be

a stationary, white Gaussian noise process with statistics  
(Ref 1):

$$E\{\mu_i\} = 0$$

$$E\{\mu_i \mu_j^T\} = R_{ij} \delta(i-j) \quad (2-12a)$$

The strength at each measurement  $j$  is given by

$$R_{ij} = \phi_{meas}^2 y_j^2 \quad (2-12b)$$

where the constant  $\phi_{meas}$  is the normalized deviation of the thermocouple measurement.

## 2.5 Summary

The mathematical description of the Space Shuttle TPS is given by the thermal model of Equation (2-1). The unknown surface heating rate due to aerodynamic forced convection is described by the enhanced heating model of equation (2-5). This new model provides a method of considering nonlinear heating rates. Additional information about the reentry environment is provided by noise corrupted thermocouple measurements obtained from the OFT program. Combining the mathematical models, set in the stochastic context of Section 2.4, with the flight test data may be accomplished through the adaptive estimation process developed in the next chapter.

### III. Identifying the Aerothermodynamic Environment

#### 3.1 Maximum Likelihood Criterion

Once the TPS-aerothermodynamic model has been formulated, the problem then becomes one of finding the "best" estimate of the aerothermodynamic environment parameters ( $\epsilon, \Delta X_A, \Phi_B, f(\rho)$ ) based on a specified trajectory estimate and thermocouple measurements. The solution of the general problem of simultaneously estimating parameters and states is developed in detail by Maybeck (Ref 15) and will serve as a basis for the solution of this particular problem. The technique described employs a maximum likelihood estimator that is found to be asymptotically sufficient and unbiased under general conditions.

The "best" estimate of the aerothermodynamic parameters at any given time is the estimate that maximizes a specified likelihood function; may be chosen, a preferable form is given as (Refs 1,15):

$$f_{\underline{u}(t_i), \underline{Y}(t_i)} \propto (\underline{\xi}, \underline{y}_i, | \theta) \quad (3-1a)$$

where (3-1a) is the joint probability function of the state,  $\underline{u}(t_i)$ , and the measurement time history,  $\underline{Y}(t_i)$ , conditioned on the parameter vector  $\underline{\xi}$ . The temperature profile at time  $t_i$  is contained in  $\underline{u}(t_i)$  and  $\underline{\xi}$  contains the set of unknown parameters. The measurement time history is given by  $\underline{Y}(t_i)$ , while  $\underline{y}_i$  is the set of realized

measurement values (Ref 1):

$$\underline{u}(t_i) = [u_1(t_i), u_2(t_i), \dots, u_n(t_i)]$$

$$\underline{Y}(t_i) = [\underline{Y}(t_1), \underline{Y}(t_2), \dots, \underline{Y}(t_i)]$$

$$\Xi = [\epsilon, \Delta X_A, \Phi_B, \text{ the parameters in } f(\rho)]$$

$$\underline{y}_i = [y_1, y_2, \dots, y_i]$$

$\xi$  and  $\theta$  are dummy values corresponding to  $\underline{u}(t_i)$  and  $\Xi$ , respectively.

The form of (3-1a) is desirable because it contains the necessary state and parameter information of other forms (Ref 15). Additionally, (3-1a) retains a dependence on initial temperature statistics which are available and lead to an improvement in estimation performance (Ref 1,15).

Through repeated applications of Bayes' rule, (3-1a) may be expressed directly as a product of Gaussian densities (Ref 1,15)

$$f_{\underline{u}(t_i), \underline{Y}(t_i) | \Xi} = f_{\underline{u}(t_i) | \underline{Y}(t_i), \Xi} \prod_{j=1}^i f_{\underline{Y}(t_j) | \underline{Y}(j-1), \Xi} \quad (3-1b)$$

Writing each density in its explicit Gaussian form motivates a redefinition of the likelihood function. By taking the natural logarithm of (3-1), the likelihood

function may be redefined as:

$$L(\xi, \theta; \underline{y}_i) = \ln f_{\underline{u}(t_i), \underline{Y}(t_i)} | \Xi (\xi, \underline{y}_i | \theta) \quad (3-2)$$

Since the natural logarithm is monotonic, the maximum of (3-1) will occur at the same values of  $\Xi$  and  $\underline{u}(t_i)$  as the maximum of (3-2). These optimal values may be found by simultaneously solving for the roots of the gradients of the likelihood equations:

$$\nabla_{\xi} L(\xi, \theta; \underline{y}_i) | \Xi \rightarrow \underline{u}^*(t_i) = 0 \quad (3-3a)$$

$$\nabla_{\theta} L(\xi, \theta; \underline{y}_i) | \Xi \rightarrow \underline{u}^*(t_i) = 0 \quad (3-3b)$$

The solution of (3-3a) may be found by substituting the Gaussian form of (3-1b) into (3-2) and solving according to (3-3a). The result is given by (Ref 1):

$$\underline{u}^*(t_i) = \hat{\underline{u}}(t_i^*) |_{\theta \rightarrow \Xi^*} = E\{\underline{u}(t_i) | \underline{Y}(t_i) = \underline{y}_i\} | \theta \rightarrow \Xi^* \quad (3-4a)$$

with associated covariance

$$\begin{aligned} P(t_i^*) |_{\theta \rightarrow \Xi^*} &= E\{(\underline{u}(t_i) - \hat{\underline{u}}(t_i)) (\underline{u}(t_i) - \hat{\underline{u}}(t_i))^T | \underline{Y}(t_i) \\ &= \underline{y}_i\} | \theta \rightarrow \Xi^* \end{aligned} \quad (3-4b)$$

Maybeck, (Ref 15), shows that this maximum likelihood estimate at time  $t_i$  is given by a Kalman filter algorithm with the optimal parameter estimate values  $\Xi^*$  replacing

the nominal parameter values in the required propagations.

Simultaneous solution of (3-3b) and (3-4a) is generally not possible in closed form, hence an iterative process must be used. This technique is developed further in Section 3.3.

### 3.2 State Estimation

Estimation of the temperature states involves solving for the conditional expectation in equations (3-4). The general theoretical development of the solution process is discussed in detail by Maybeck (Ref 15) and Jazwinski (Ref 12). The resulting Kalman filter algorithm is presented here with specific equations relevant to the estimation of the temperature profile.

The nonlinear nature of the combined thermal/heating model dictates the use of a (nonlinear) extended Kalman filter for state propagation as follows. Given the a posteriori statistics

$$\hat{\underline{u}}(t_i^+) \triangleq E \{ \underline{u}(t_i) | \underline{Y}(t_i) = \underline{y}_i \} \quad (3-5a)$$

$$P(t_i^+) \triangleq E \{ (\underline{u}(t_i) - \hat{\underline{u}}(t_i)) (\underline{u}(t_i) - \hat{\underline{u}}(t_i))^T | \underline{Y}(t_i) = \underline{y}_i \} \quad (3-5b)$$

the a priori expectation

$$\hat{\underline{u}}(t_{i+1}^-) \triangleq E \{ \underline{u}(t_{i+1}) | \underline{Y}(t_i) = \underline{y}_i \}$$

is approximated by solving

$$\hat{\underline{u}}(t) = F(\hat{\underline{u}}(t), q_r(t), f(\rho); \Xi) \quad (3-6)$$

on the interval  $t_i \leq t \leq t_{i+1}$ . The differential equation is initialized at each time  $t_i$  by  $\hat{\underline{u}}(t_i) = \hat{\underline{u}}(t_i^+)$  as provided by the previous measurement update. Equations (3-6) represents the differential equation of the thermal model as given by (2-1). These equations are solved numerically as described in Chapter II.

The priori covariance is found by the matrix equation

$$P(t_{i+1}^-) = \Phi\{t_{i+1}, t_i; \hat{\underline{u}}(t_i^+)\} P(t_i^+) \Phi\{t_{i+1}, t_i; \hat{\underline{u}}(t_i^+)\} \\ + \int_{t_i}^{t_{i+1}} \Phi\{t_{i+1}, t; \hat{\underline{u}}(t_i^+)\} Q(t) \Phi\{t_{i+1}, t; \hat{\underline{u}}(t_i^+)\} dt \quad (3-7)$$

where  $\Phi\{\cdot\}$  is the state transition matrix derived from the linearized model (2-8) of equations (2-1) evaluated at  $\hat{\underline{u}}(t_i^+)$  (as an approximation for  $\hat{\underline{u}}(t/t_i)$  for  $t \in [t_i, t_{i+1}]$ ) (Ref 1):

$$\dot{\Phi}\{t_i y; \hat{\underline{u}}(t_i^+)\} = L\{t; \hat{\underline{u}}(t_i^+)\} \Phi\{t, y; \hat{\underline{u}}(t_i^+)\} \\ L\{t; \hat{\underline{u}}(t_i^+)\} \stackrel{\Delta}{=} \nabla_u F(\underline{u}(t), q_r(t), f(\rho); \theta) |_{\substack{\underline{u}(t) = \hat{\underline{u}}(t_i^+) \\ \theta = \Xi^*}}$$

Sagstetter (Ref 20) presents the details of the numerical solution of equation (3-7) to obtain an approximate a priori covariance.

The a posteriori expectation,  $\hat{\underline{u}}(t_{i+1}^+)$ , and covariance,

$P(t_{i+1}^+)$ , are determined by optimally combining the a priori value with the measurements taken at time  $t_{i+1}$ . Since the measurement process is linear, the Kalman update equations reduce to those of a linear Kalman filter

$$\hat{\underline{u}}(t_{i+1}^+) = \hat{\underline{u}}(t_{i+1}^-) + K(t_{i+1}) \{ \underline{y}_{i+1} - H \hat{\underline{u}}(t_{i+1}^-) \} \quad (3-8)$$

where the Kalman gain,  $K(t_{i+1})$ , is given by

$$K(t_{i+1}) = P(t_{i+1}^-)^T \{ H P(t_{i+1}^-) H^T + R \}^{-1} \quad (3-9)$$

The a posteriori covariance is given by the Joseph form as

$$\begin{aligned} P(t_{i+1}^+) &= \{ I - K(t_{i+1}) H \} P(t_{i+1}^-) \{ I - K(t_{i+1}) H \}^T \\ &\quad + K(t_{i+1}) P(t_{i+1}^-) K^T(t_{i+1}) \end{aligned} \quad (3-10)$$

It should be noted that the approximate a priori covariance obtained through the use of the linearized state transition matrix influences the a posteriori expectation through the Kalman gain (3-9). The Joseph form is used in the update equation because it is less sensitive to errors in this Kalman gain than the standard form (Ref 15). In addition, the symmetric properties of the additive matrices in (3-10) provide better conditioned numerical computations (Ref 15).

The equations used to generate the expectation, (3-6)

and (3-8), assume known values for the parameters  $\Sigma$ . The estimator thus uses the best estimate of  $\Sigma$  currently available from the parameter estimation scheme described in the next section.

### 3.3 Parameter Estimation

As stated previously, the solution of equations (3-3) resulting from the likelihood equations must be solved using an iterative process. A Newton-Raphson technique can be used to generate a solution for the unknown parameters in terms of the previous best estimate (Ref 15)

$$\hat{\theta}^*(t_i) = \hat{\theta}_*(t_i) - \frac{\partial^2 L\{\hat{u}_*(t_i), \hat{\theta}_*(t_i); y_i\}}{\partial \theta^2}^{-1} \cdot \frac{\partial L\{\hat{u}_*(t_i), \hat{\theta}_*(t_i); y_i\}}{\partial \theta}^T \quad (3-11)$$

where  $L\{\hat{u}_*(t_i), \hat{\theta}_*(t_i); y_i\}$  is the likelihood function using the best estimate of the temperature profile from the Kalman estimator ( $\hat{u}_*(t_i)$ ) and the previous best parameter estimate ( $\hat{\theta}_*(t_i)$ ). The matrix of mixed second partial derivatives, or Hessian, in (3-11) must be of full rank for the inversion process. Even so, the inversion of the Hessian matrix causes the computational burden to be enormous.

Rao provides an approximation called "scoring" which

reduces computation and maintains accuracy as long as the number of samples is large (Refs 1,9,15). The approximation is that

$$\frac{\partial^2 L\{\hat{u}_*(t_i), \hat{\theta}_*(t_i); y_i\}}{\partial \theta^2} \underset{\sim}{=} -J\{t_i, \hat{u}_*(t_i), \hat{\theta}_*(t_i)\} \quad (3-12)$$

where  $J\{\cdot\}$  is called the conditional information matrix and is given by

$$J\{t_i, \hat{u}_*(t_i), \hat{\theta}_*(t_i)\} \stackrel{\Delta}{=} E\{\nabla_{\theta} L\{\hat{u}_*(t_i), \theta; y_i\} \nabla_{\theta} L\{\hat{u}_*(t_i), \theta; y_i\}^T |_{\theta = \hat{\theta}_*}\} \quad (3-13)$$

In fact, it can be shown that (Ref 15)

$$-J\{t_i; \hat{\theta}_*(t_i)\} = E\left\{\frac{\partial^2 L\{\hat{u}_*(t_i), \theta; y_i\}}{\partial \theta^2} \Big|_{\theta = \hat{\theta}_*}\right\}$$

so that the approximation of the Hessian for a given measurement can well be approximated by its ensemble average over all possible measurement time histories. With the approximation (3-12), equation (3-11) now becomes

$$\begin{aligned} \hat{\theta}_*(t_i) &= \hat{\theta}_*(t_i) + J\{t_i, \hat{u}_*(t_i), \hat{\theta}_*(t_i)\}^{-1} \\ &\quad \frac{\partial L\{\hat{u}_*(t_i), \hat{\theta}_*(t_i); y_i\}^T}{\partial \theta} \end{aligned} \quad (3-14)$$

It can be shown that the  $k_{th}$  element of the gradient term in (3-14) can be given as (Ref 1)

$$\frac{\partial L\{\hat{u}_*(t_i), \hat{\theta}_*(t_i); \underline{y}_i\}}{\partial \theta_k} = \sum_{j=1}^i \frac{\partial \hat{u}(t_j^-)}{\partial \theta_k} H^T \{HP(t_j^-)H^T + R\}^{-1} \\ x\{\underline{y}_i - \hat{H}\hat{u}(t_j^-)\} \quad (3-15)$$

The  $k_{th}$  element of the conditional information matrix may be approximated as

$$J_{kl} = \sum_{j=1}^i \frac{\partial \hat{u}(t_j^-)}{\partial \theta_k} H^T \{HP(t_j^-)H^T + R\}^{-1} H \frac{\partial \hat{u}(t_j^-)}{\partial \theta_l} \quad (3-16)$$

The a priori sensitivity,  $\hat{u}_{\theta_k}(t_j^-)$ , is found by taking the partial derivatives of (2-1) with respect to the parameter vector for the time interval of interest:

$$\dot{\hat{u}}_{\theta_k} = C_k \hat{u}_{\theta_k} + D_k \quad (3-17a)$$

The a posteriori sensitivity state,  $\hat{u}_{\theta_k}(t_j^+)$ , is obtained by taking the partial derivatives of (3-8) with respect to  $\theta_k$  and is found to be (Ref 15):

$$\dot{\hat{u}}_{\theta_k}(t_j) = \{I - K(t_j)H\} \{\hat{u}_{\theta_k}(t_j^-) + \frac{\partial P(t_j^-)}{\partial \theta_k} \\ \times \{H^T(HP(t_j^-)H^T + R)^{-1} (\underline{y}_j - \hat{H}\hat{u}(t_j^-))\}$$

Audley (Ref 1) argues that this equation may be simplified by assuming

$$\frac{\partial P(t_j^-)}{\partial \theta_k} = 0 \quad \text{and} \quad \frac{\partial P(t_j^+)}{\partial \theta_k} = 0$$

It can be argued that these terms contribute nothing to a valid means of estimating parameters because the conditional information matrix includes these partials only in terms that are not dependent on the measurement values (Ref 1). With this assumption, the a posteriori sensitivity reduces to

$$\hat{u}_{\theta_k}(t_j^+) = \{I - K(t_j)H\} \hat{u}_{\theta_k}(t_j^-) \quad (3-17b)$$

Maybeck (Ref 15) arrives at the same form as (3-17b) by neglecting less sensitive terms and retaining only the highly sensitive weighted least squares type terms.

The sensitivities are calculated throughout the measurement time history so as to update the running score vector and the conditional information matrix. With this information, an optimal estimate may be found using (3-14).

Information regarding the uncertainty of the parameter estimates found from (3-14) may be found from the Cramer-Rao inequality (Ref 1,2,5,15). In the case of unbiased estimates, this inequality relates the conditional information matrix to the covariance of the parameter estimate.

$$\text{cov} \{\hat{\theta}^*\} = E\{ (\hat{\theta}^* - \theta_t) (\hat{\theta}^* - \theta_t)^T \} \geq J_{t_i, \hat{u}_*(t_i), \hat{\theta}_*}^{-1} \quad (3-18)$$

where  $\theta_t$  is the true value of the parameter vector. Thus the inverse of the conditional information matrix as approximated by (3-12) can be used to construct a lower bound for the uncertainties in the parameter estimates.

### 3.4 Algorithm Summary

The operational algorithm incorporating the state and parameter estimators as developed in this chapter is summarized by Figure 4 and serves as a basis for the HEATEST program. The primary mode of operation is to process recursively a short segment of the reentry trajectory. Transient flight test maneuvers of short duration (30-90 seconds) provide data which is processed to yield estimates of model parameters as follows.

Initial conditions for the temperature profile,  $u(t_0)$ , are either specified or obtained by processing data up to the start of the transient maneuver, while the initial covariance,  $P(t_0)$ , is specified at maneuver start. Initial sensitivities of the state are specified to be zero or are obtained from prior processing. The state estimates, covariance, and sensitivities can be solved

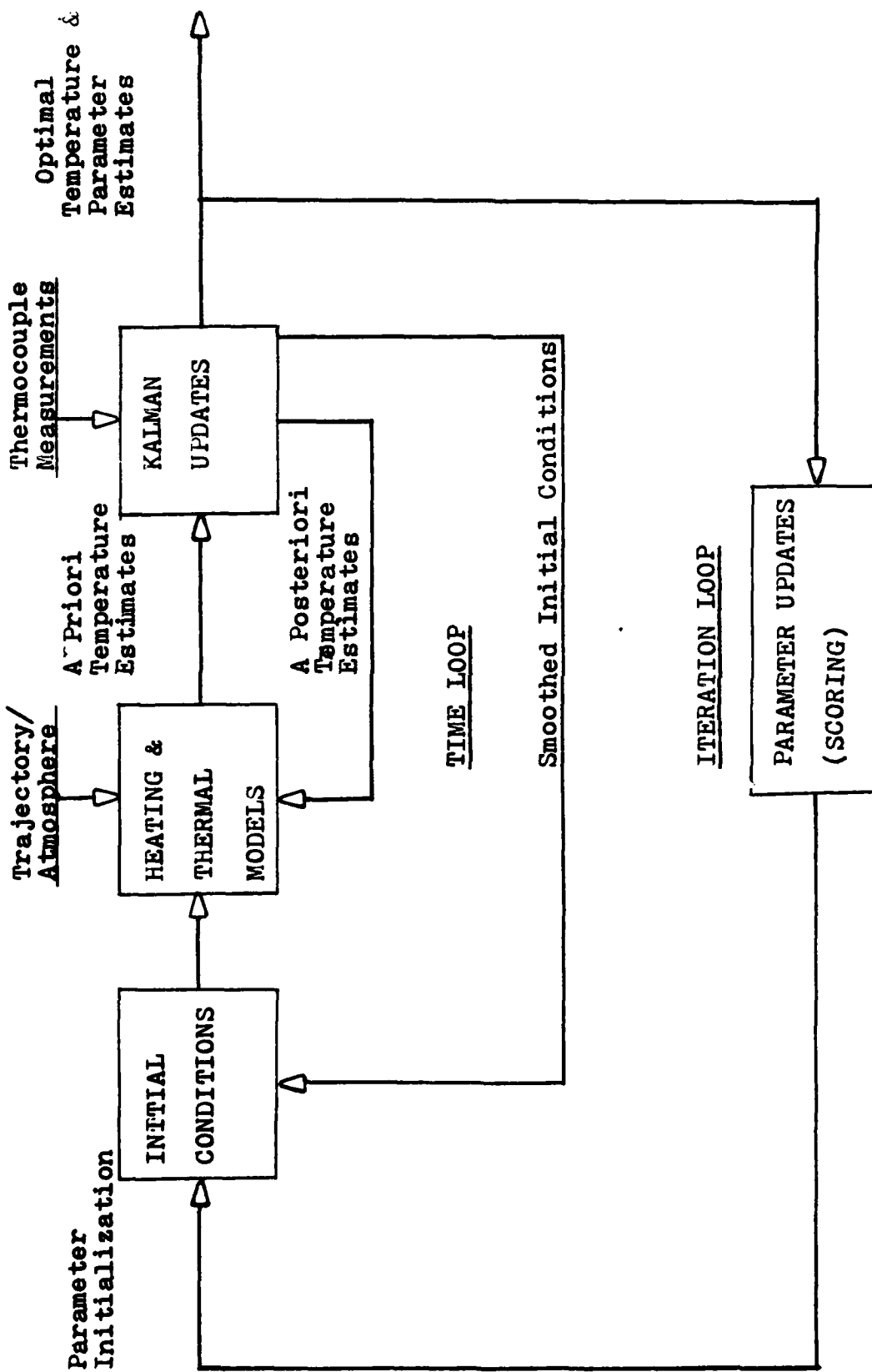


Figure 4. HEATEST Data Reduction with Initial Condition Smoothing

throughout the maneuver history by incorporating the measurement data. The value for the unknown parameter vector,  $\Xi$ , is the best prior value, either from the previous pass through the maneuver data, a preflight value, or a value generated in conjunction with the initial conditions.

Once the maneuver data has been processed, a new estimate may be found for the parameter vector. Since the estimate is based only on the singly processed maneuver, repeated iterations are necessary for convergence to some optimal estimate,  $\hat{\theta}_* \rightarrow \hat{\theta}^*$ .

As an improvement to the original algorithm, initial conditions may be processed with each iteration through a smoothing estimator which enhances the initial values based on the maneuver data. This estimator, which can be used to backward-process measurements from  $t_f$  to  $t_o$ , is developed in detail in the next chapter.

#### IV. Initial Condition Smoothing

##### 4.1 Smoothing Techniques

Results using the HEATEST program have sometimes been affected by the imprecise manner in which the initial conditions are generated (Ref 8). To alleviate this problem, Audley and Hodge (Ref 1) suggest the incorporation of some type of smoothing algorithm to enhance initial values of  $\underline{u}(t_0)$  and  $P(t_0)$  based on the maneuver data.

The general smoothing problem is that of predicting the state at any given time based on "future" measurements, in addition to the past and present measurements normally considered in a conventional filter. Thus, the state estimation scheme incorporates measurements from the entire history. More detail on the general smoothing problem is given by Maybeck (Ref 15), Meditch (Ref 16), and Fraser (Ref 6). Although there exist many classes of smoothers, two were considered for implementation in the HEATEST program: the "fixed-interval smoother", for smoothing the state estimates throughout the measurement history; and the "fixed-point smoother", for smoothing only the initial states.

Fraser (Ref 6) shows the general fixed-interval smoother to be a combination of two optimal filters. A

forward filter, formulated as the standard filter already implemented in the identification algorithm, would calculate state estimates based on measurements from the initial time,  $t_o$ , to the current time,  $t_i$ :

$$\hat{\underline{u}}(t_i^+) = E\{\underline{u}(t_i) | \underline{y}(t_1, t_i) = \underline{y}_{1,i}\} \quad (4-1)$$

A backward filter is run independently from the final condition,  $t_f$ , to time  $t_i$ , so as to incorporate "future" measurements

$$\hat{\underline{u}}_b(t_i^-) = E\{\underline{u}(t_i) | \underline{y}(t_{i+1}, t_f) = \underline{y}_{i+1,f}\} \quad (4-2)$$

where the notation  $\hat{\underline{u}}_b(t_i^-)$  denotes the estimate of  $\hat{\underline{u}}$  provided by the backward filter just before the measurement at time  $t_i$  is incorporated. The results from these two filters are then combined in an optimal manner so as to provide a smoothed state estimate at time  $t_i$ . "Better" state estimates throughout the measurement history would be expected due to the smoothing process.

A fixed-point smoother, rather than smoothing the states at each point in time, is constructed so as to smooth only one point in time at which the values of the system state is considered critical; i.e. the initial time for the problem at hand. A forward filter is run in the same manner as the forward filter described above,

but as new data becomes available, the measurement information is propagated back to the critical point (initial condition) to provide an updated (smoothed) estimate

$$\hat{\underline{u}}(t_o/t_j) = E\{\underline{u}(t_o) | \underline{y}(t_j) = \underline{y}_j\} \quad t_j = t_o, t_1, \dots, t_f \quad (4-3)$$

Ideally, to solve this particular problem, the backward propagation of information for either smoother would incorporate a nonlinear or extended filter of the form used in the forward propagation (Section 3.2). However, the solution of Equation (2-1) backward in time has been shown to have unstable properties and in general is difficult to solve (see Appendix B for a further discussion). Therefore, the linearized form of the state transition matrix given in Equation (2-8) will be used. Development of both smoothers incorporates this form and is described in the following sections.

#### 4.2 Fixed-Interval Smoothing

Maybeck (Ref 15) provides details of the development of the fixed-interval smoother which will be summarized here. First, the forward filter is applied up to the current time,  $t_i$ , incorporating the measurement to provide a state estimate,  $\hat{\underline{u}}(t_i^+)$ . The existing extended Kalman filter described in Chapter II can be used for this

purpose.

An independent backward-running filter may be formulated as an inverse covariance form. This form provides a priori statistics at the final time,  $t_f$ , that cannot be obtained by the conventional form. Additionally, this form insures stability of the backward filter (provided the linearized state transition matrix is used) since the forward filter is stable. If the states in the backward direction are denoted  $\hat{\underline{u}}_b(t_i)$  and  $P_b(t_i)$ , then the inverse covariance form is given as  $\hat{\underline{x}}_b = P_b^{-1} \hat{\underline{u}}_b$  and  $P_b^{-1}(t_i)$ . Initialization occurs at the final time as given by

$$\hat{\underline{x}}_b(t_f^-) = 0 \quad (4-4a)$$

$$P_b^{-1}(t_f^-) = 0 \quad (4-4b)$$

Estimation propagation backwards in time to the preceding measurement time is given by

$$\hat{\underline{x}}_b(t_{k-1}^-) = \Phi^T(t_k, t_{k-1}) L(t_k) \{ \hat{\underline{x}}_b(t_k^+) B(t_{k-1}) \} \quad (4-5a)$$

$$\begin{aligned} P_b^{-1}(t_{k-1}^-) = & \Phi^T(t_k, t_{k-1}) \{ L(t_k) P_b^{-1}(t_k^+) L^T(t_k) \\ & + J(t_k) Q^{-1} J^T(t_k) \} \Phi(t_k, t_{k-1}) \end{aligned} \quad (4-5b)$$

where

$$J(t_k) = P_b^{-1}(t_k^+) \{ P_b^{-1}(t_k^+) + Q^{-1} \}^{-1} \quad (4-5c)$$

$$L(t_k) = I - J(t_k) \quad (4-5d)$$

The time indices on the state transition matrices indicate backward propagation of adjoint system relations. Measurement updates of the backward filter are generated by

$$\hat{x}_b(t_k^+) = \hat{x}_b(t_k^-) + H^T R^{-1} y_i \quad (4-6a)$$

$$P_b^{-1}(t_k) = P_b^{-1}(t_k^-) + H^T R^{-1} H \quad (4-6b)$$

Equations (4-5) and (4-6) are recursively for  $k=f, (f-1), \dots, (i+1)$  to generate  $\hat{x}_b(t_i^-)$ .

Combining the estimates from the forward filter,  $\hat{u}(t_i^-)$  and  $P(t_i^+)$ , and those of the backward filter,  $\hat{x}_b(t_i^-)$  and  $P_b(t_i^-)$ , can be accomplished by

$$\hat{u}(t_i/t_f) = X(t_i) \hat{u}(t_i^+) + P(t_i/t_f) \hat{x}_b(t_i^-) \quad (4-7a)$$

$$P(t_i/t_f) = Z(t_i) P(t_i^+) Z^T(t_i) + W(t_i) P_b^{-1}(t_i^-) W^T(t_i^-) \quad (4-7b)$$

where

$$X(t_i) = \{I + P(t_i^+) P_b^{-1}(t_i^-)\}^{-1} \quad (4-7c)$$

$$W(t_i) = P(t_i^+) X^T(t_i) \quad (4-7d)$$

$$Z(t_i) = I - W(t_i) P_b^{-1}(t_i^-) \quad (4-7e)$$

The optimal smoothed estimates are now given by  $\hat{u}(t_i/t_f)$

and  $P(t_i/t_f)$ . Computationally, this process can be achieved by first running the backward filter over the entire interval and storing values of  $\hat{x}_b(t_k^-)$  and  $P_b^{-1}(t_k^-)$ . Next, the forward filter is run simultaneously with the smoother relations of (4-7) thus generating smoothed estimates at each sample time,  $\hat{u}(t_i/t_f)$  and  $P(t_i/t_f)$ .

#### 4.3 Fixed-Point Smoothing

The optimal fixed-point smoother for a general point is given by Meditch (Ref 16) and Maybeck (Ref 15). The smoother relation is run concurrently with the Kalman filter of Section 3.2 and is given by

$$\hat{u}(t_o/t_j) = \hat{u}(t_o/t_{j-1}) + W(t_j) K(t_j) \{y_j - H \hat{u}(t_j^-)\} \quad (4-8)$$

where  $\hat{u}(t_o/t_j)$  is the smoothed initial state based on measurements through time  $t_j$ ;  $\hat{u}(t_j^-)$  and  $\hat{u}(t_j^+)$  are the a priori and a posteriori values of the state at time  $t_j$  as obtained from the Kalman filter;  $y_j$  is the measurement at time  $t_j$ ;  $H$  is the measurement matrix given by (2-11); and  $K(t_j)$  is the Kalman gain matrix given by (3-9). Equation (4-8) includes a residual term,  $\{y_j - H \hat{u}(t_j^-)\}$ , available directly from the existing forward filter (3-8). Thus it can be interpreted as a means of "reflecting back" the information contained in the filter residual at each time  $t_j$  about the initial state value at time,  $t_o$  (Ref 15).

The smoother gain matrix  $W(t_j)$  is defined to be

$$W(t_j) \stackrel{\Delta}{=} \prod_{k=0}^{j-1} A(t_k) = W(t_{j-1}) A(t_{j-1}) \quad (4-9a)$$

$$A(t_k) \stackrel{\Delta}{=} P(t_k) \Phi(t_{k+1}, t_k) P^{-1}(t_{k+1}) \quad (4-9b)$$

where  $\Phi$  is the linearized transition matrix; and  $P(t_k^+)$  and  $P(t_{k+1}^-)$  are the a posteriori and a priori covariance at time  $t_k$  and  $t_{k+1}$  respectively.

An approximation for the error committed by this estimator,  $\hat{u}(t_0) - \hat{u}(t_0/t_j)$ , is to consider it Gaussian and zero mean for all  $j$ , with covariance

$$P(t_0/t_j) = P(t_0/t_{j-1}) + W(t_j) \{P(t_j^+) - P(t_j^-)\} W^T(t_j) \quad (4-10a)$$

or

$$P(t_0/t_j) = P(t_0/t_{j-1}) - W(t_j) K(t_j) H P(t_j^-) W^T(t_j) \quad (4-10b)$$

The smoothing algorithm is initialized by

$$\hat{u}(t_0/t_0) = \hat{u}(t_0) = \underline{u}_0 \quad (4-11a)$$

$$P(t_0/t_0) = P(t_0) \quad (4-11b)$$

To avoid the inversion of the  $n \times n$  matrix,  $P(t_j)$ , of Equation (4-9b), Fraser (Ref 6) provides an alternative form which requires only the inversion of the  $m \times m$  diagonal matrix  $R$  of (2-12),

$$\hat{\underline{u}}(t_0/t_j) = \hat{\underline{u}}(t_0/t_{j-1}) + W(t_j) H^T R^{-1} \{ \underline{y}_j - \hat{H}\hat{\underline{u}}(t_j^-) \} \quad (4-12)$$

where  $W(t_j)$  is now generated by means of the recursion

$$W(t_j) = W(t_{j-1}) \Phi(t_j, t_{j-1}) \{ I - S(t_j) P(t_j^+) \} \quad (4-13a)$$

$$S(t_j) = H^T R^{-1} H \quad (4-13b)$$

starting from

$$W(t_0) = P(t_0) \quad (4-13c)$$

Again the residual term available from the forward filter is found in Equation (4-12) and provides the means for reflecting measurement information back to the initial time.

The error covariance can be computed as

$$\begin{aligned} P(t_0/t_j) &= P(t_0/t_{j-1}) - W(t_j) \{ S(t_j) P(t_j^-) S(t_j) \} \\ &\quad + S(t_j) W^T(t_j) \end{aligned} \quad (4-14)$$

The smoother algorithm is initialized by Equation (4-11).

#### 4.4 Smoothing Algorithm

Although the fixed-interval smoother provides smoothed estimates throughout the time history, it adds a significant amount of computational complexity when compared with the fixed-point smoother. For the HEATEST Program, this is a major concern. The main objective is to find better estimates of the initial conditions, and since the

existing Kalman filter provides satisfactory estimates throughout the rest of the time history, a fixed-point smoother is adequate. Thus the Fraser fixed-point smoother of Equations (4-12) - (4-14) has been incorporated into the estimation algorithm.

An important consideration in the operation of this smoother is the length of the smoothing interval. Because of the use of the linearized state transition matrix to reflect information backwards, errors caused by this approximation and other model uncertainties may increase if smoothing is conducted over a long time interval. Thus, it may be necessary to restrict the number of sample measurements that are included for smoothing.

One criterion for the smoothing interval may be the RC time constant analogy mentioned in (2-7). The approximation is that a step input in the heating rate at the surface will propagate to the interior according to

$$RC_l = \rho_l c_l x_l^2 / K_l$$

where the RC time constant,  $RC_l$ , is in units of seconds and  $x_l$  is now the distance from the surface. A node is expected to reach 98% of its asymptotic temperature within an amount of time given by three time constants using this

analogy. Since the heating rate at the surface is actually nonlinear, smoothing beyond a time interval described by this time constant serves to propagate errors from the linear state transition matrix assumption. Thus a smoothing interval of three time constants is used for the smoothing interval at each node point.

Perhaps a better alternative may be to consider the eigenvalues of the system for calculating the smoothing interval. However, since the Schur method of decomposition is used for calculating the state transition matrix (Ref 20), the eigenvalues are not directly available from the program. The added burden of calculating these eigenvalues is unwarranted for this application.

Operationally, the updated HEATEST Program provides an option to use this time constant analogy or to specify a desired interval. Additionally, the smoother may be "shut off" completely when initial condition smoothing is not desired.

#### 4.5 Summary

The fixed-point smoother algorithm provides an efficient and computationally tractable method for estimating the TPS temperature profile at the start of a given maneuver. Incorporation of this smoother into the adaptive estimation scheme is shown in Figure 4. The current HEATEST program now contains this smoother, as

well as the enhanced heating model described in Chapter II. Testing and application of the improved scheme is described in the next chapter, along with analyses of the results.

## V. RESULTS

### 5.1 Approach

To validate the improvements incorporated into the HEATEST estimation scheme, it is necessary to apply the program to realistic simulations and actual flight data. Simulated thermocouple measurements can be generated for specified heating models and initial conditions. With the true value for the parameters and initial condition known, a simulated estimation using the updated HEATEST program can be compared to the known values. Additionally, linear and nonlinear forms of the heating model may be contrasted to show the flexibility of the new form. For flight data, verification of the enhanced heating model can be continued by applying it to STS-2 lower surface measurements where previous results are adequate and available. Since the lower surface is expected to have a linear heating rate, similar results should be obtained with both linear and nonlinear models. STS-2 OMS pod data provides a good opportunity to apply the scheme to an area with a nonlinear heating rate. The new model also enables a further investigation of the time skew problem due to the possible nonisothermal wall effect on the OMS pod. For initial condition estimation, simulations with known initial conditions can also be conducted and the RC time constant approximation for the smoothing interval can be

verified. Application of the smoother to STS-4 lower surface data, where a telemetered data loss occurred and initial conditions are uncertain, can provide information concerning a possible Reynolds number or Mach effect during the Mach 12 POPU maneuver.

The results for these cases, given in Appendices C - F, include parameter and state estimates, along with some measure of their uncertainty or accuracy. For parameter estimates, an uncertainty bound is derived from the Cramer-Rao Bound described by Equation (3-18). Thus, this does not represent an absolute measure of uncertainty, but can be used for comparison purposes. For state estimates, an average error is presented which represents the average deviation of measurements and a priori estimates. This describes how well the model "fits" the thermocouple data. Because thermocouple accuracies vary for each flight condition and location on the Orbiter, this measure is useful only for comparisons of runs made with the same data. Finally, uncertainties of smoothed initial conditions are described by the variance, which is calculated from the smoothed error covariance matrix.

Two types of thermal models were used in obtaining these results. The lower surface model includes a plug of thirteen node points with thermocouples located at node points 2, 5, 8, 11, and 13. The OMS pod includes ten node points with only

a surface thermocouple located just under the coating thickness at node 2. For both models, thermocouples provide measurements at a sample rate of one per second.

### 5.2 Heating Model Simulation

The lower surface thermal model was combined with two segment and three segment heating models to generate a non-linear response, similar to that which might be observed on the OMS pod. Trajectories from the STS-2 Mach 20 Pushover Pullup maneuver were used to generate the simulated thermocouple data. Eight-bit word noise of the temperature data was not simulated, but could be added for an even more realistic simulation. Results described in this section are given in Appendix C.

Simulated thermocouple data, along with the a priori temperature estimates of the HEATEST program, are given in Figure C.1 for the two segment model simulation. The predicted heating model is depicted in Figure C.2. These parameter estimates, as shown in Table C-1, provide good agreement with the actual specified values. Any discrepancy may be attributed to approximate initial conditions that were used for the estimated case.

Exact initial conditions were used for a three segment model simulation and the results shown provide better accuracy. For this model, one, two, and three segment estimates were

obtained as given in Table C-2. It should be noted that the heating derivatives represent slopes of each linear segment and as such cannot be compared directly for different models. Rather, the heating ratio itself at specified angles of attack should be contrasted for the various models, as depicted by Figure C.4. As expected, the multiple segment models provide more accurate results as indicated by the average error of Table C-2, with the three segment model predicting the specified values exactly. However, parameter uncertainty bounds tend to increase with the multiple segment models. This can be attributed to the approximation used for calculating the sensitivities at the knots or break points, as well as an increase in the number of parameter estimates or "degrees of freedom" of the scheme. The high uncertainties of the break point estimations for the three segment case indicate that difficulties may be encountered when estimating these points with noisy data and rapid transients. By fixing these points and thus reducing the number of estimated parameters, uncertainty bounds decreased by 50 - 55% (Table C-2.B.).

Another important result shown in Table C-2 concerns the coating thickness of the one segment estimation case. A larger coating thickness with a high uncertainty bound is predicted for the nonlinear data used. This implies that the linear perturbation model attempts to account for non-linear heating ratios by estimating a larger coating thickness.

This would explain some of the large coating thicknesses obtained in previous flight data results (Ref 7,8,9). By specifying the coating thickness, as in Table C-2.B., a smaller average error may be obtained.

Figure C.4 provides a graphic comparison of the one, two, and three segment estimations of the three segment model. The one segment interpolation represents the linear perturbation model assumption as contained in the original HEATEST program. This model attempts a linear best fit, which can be grossly inaccurate for highly nonlinear heating rates. Multiple segment piecewise linear models provide a much better fit as shown in Figure C.4.

### 5.3 Heating Model Flight Data

The updated heating model was applied to STS-2 flight data at the Mach 20 Pushover Pullup (POPU) maneuver for both the lower surface and OMS pod. Results for these cases are given in Appendix D.

The heating ratio for the lower surface is expected to be fairly linear with changes in angle of attack (Ref 10). Results from STS-2 data using the linear perturbation model have been good (Ref 7). Application of the multiple segment interpolation model should reproduce this result. Figure D.2 compares the heating ratio estimated assuming one, two, and three segment models. The results are similar and the multiple

segment models predict an essentially linear heating ratio. This proves the validity of the linear perturbation assumption for the lower surface.

In previous analyses of the OMS pod, nonlinearities were accommodated by processing the data in small time segments (Ref 7). Typical results are shown by Figure D.4, which uses data processed in four time increments. This figure shows that the linear perturbation assumption is not valid throughout the entire maneuver. The entire maneuver can be processed, however, by applying the new heating model. Two and three segment interpolation models were used for the heating ratio estimates given by Figures D.5, D.6, and Table D-2. Results obtained with these models agree well with previous results. In general, improved performance is obtained from the interpolation forms. The average error of the three segment model shows a 10% improvement over that of the original model, while the two segment model shows a 30% decrease. The better performance of the two segment model over the three segment model can be attributed to a reduction in the number of estimated parameters and the adequacy of the two segment form.

A major problem in previous OMS pod results was the identification of a three second time skew, which may be caused by the nonisothermal wall effect (Ref 9). Thermocouple samples were lagged by three seconds to enable data

correlation and eliminate hysteresis in the heating ratio profile. An investigation of this problem was conducted using the new heating model. The advantage of the new model in investigating this problem is that an estimate for the coating thickness may be obtained for the entire maneuver interval and data correlation is easier.

Table D-3 compares heating parameter estimates for various time skews using a two segment model. For adequate results, it was necessary to estimate the coating thickness,  $\Delta X_A$ , and the sideslip heating derivative,  $q_\beta$ . Figure D.7 shows the increase in heating with decreasing time skews. Figure D.8 compares estimated coating thickness, as well as sideslip heating derivatives, for various time skews. Unusually high coating thickness predictions were obtained for smaller skews. Although large thicknesses may be expected due to repairs of the OMS pod prior to STS-2 (Ref 9), estimations for zero and one second skews are unreasonable. Thus, time skews are shown to be necessary for reasonable prediction of the coating thickness. In addition, the estimated sideslip heating derivative,  $q_\beta$ , decreases with time skew as does the uncertainty of the predictions.

Since an approximate value for the coating thickness for this flight was virtually unknown a priori, the magnitude of the necessary time skew is difficult to determine. To identify the magnitude of the time skew, the average errors of

temperature predictions for various time skews are shown in Figure D.9. Although previous analysis has indicated a three second skew, this figure indicates that a two second skew may be desirable. The coating thickness predicted by a two second skew is high, but may not be unreasonable. A conservative approach may be to identify the time skew as having a range of possible values from two to four seconds.

#### 5.4 Simulation With Initial Condition Estimation

For testing the fixed-point initial condition smoother, a simulation of STS-4 lower surface data with known initial conditions was generated (Figure E.1). Poor initial conditions were used to initialize the smoother and final smoothed conditions at each node were compared to the actual initial temperature values. Simultaneous parameter estimation was conducted to evaluate the feasibility of using the smoother in an adaptive estimation setting.

Table E-1 shows the final smoothed conditions after six parameter iterations. In addition, the final parameter estimates are shown. Comparison to the actual model and initial conditions is excellent and provides confidence in the validity of the smoother.

To analyze smoother performance more explicitly, Figures E.2 and E.3 indicate the degree of smoothing with increasing sample periods for the first parameter iteration. For thermocouple node points (Figure E.2), the smoother quickly

converges to the final smoothed values. For node points without a thermocouple, convergence is much slower, but well within the three time constant approximation. This indicates the validity of using this approximation for calculating the smoothing interval. Also, as expected, more confidence is obtained for thermocouple node points as indicated by the smoothed variance values.

### 5.5 Flight Results With Initial Condition Estimation

An important application of the initial condition smoother is to analyze the data from the lower surface of the STS-4 Mach 12 Pushover Pullup maneuver. Previous analyses of this data (Refs 1,7,8) have indicated lower heating derivatives for the STS-4 data than obtained for the STS-2 Mach 20 maneuver data. Loss of telemetered data from the beginning to the middle of the maneuver complicate the analysis. It has been determined that transitions to turbulent flow and then back to laminar flow occurred during this data loss (Refs 1, 7,8). However, it is unknown whether the lower heating ratio estimates are a result from some unmodeled Mach or Reynolds number effect or from inaccurate initial conditions at the start of the processed data. Audley and Hodge (Ref 1) indicate that an initial condition smoother would resolve this discrepancy.

Thermocouple data processed in the middle of the maneuver is presented in Figure F.1. Smoothing was applied to the

approximate initial conditions used in previous analyses. Convergence for the smoothed initial temperatures, shown in Table F-1, was obtained. The higher temperatures just below the surface (Figure F.2) indicate heat storage that would be consistent with flow transitions. Although overall comparison of the heating ratio estimates from STS-2/STS-4 during laminar flow remains favorable, lower heating derivatives are still predicted for the STS-4 maneuver (see Figure F.3). This, then does indicate the presence of an unmodeled Mach or Reynolds number effect, since the uncertainties about the initial conditions have essentially been eliminated.

### 5.6 Summary

Results from both simulated and actual flight data show the flexibility and accuracy of the improved HEATEST program. Both the nonlinear heating model and the fixed-point initial condition smoother demonstrate excellent performance characteristics. A summary of the important conclusions gained from the results of this chapter, as well as recommendations for further improvements and future applications of this scheme, are provided in the following chapter.

## VI. CONCLUSIONS AND RECOMMENDATIONS

### 6.1 Conclusions

Areas on the Space Shuttle Orbiter with nonlinear heating rates may be successfully modeled by a piecewise linear interpolation scheme. The feasibility of this model has been demonstrated through applications to both simulated and actual flight data. Problems may arise when estimating multiple knots (break points) due to the approximation of the sensitivity calculations at these locations. To avoid such difficulties, these locations may be specified rather than estimated and accurate results can be obtained.

Simultaneous smoothing of initial conditions with the adaptive estimation scheme successfully provides better estimates of temperatures at maneuver start and enhances the overall estimation process. In cases of data loss prior to maneuver start, initial conditions can now be estimated based on "future" data obtained after the initial time. Use of the RC time constant approximation, as shown by simulated cases, provides a feasible method of calculating the smoothing interval.

Applications of the new program incorporating both the nonlinear heating model and fixed-point initial condition smoother have provided some useful and important results. From simulated data, it has been determined that the original linear perturbation heating model may estimate high values

for the coating thickness when applied to an area with a non-linear heating rate. Use of the improved model provides better estimates with lower uncertainties in such cases.

OMS pod data from STS-2 can now be processed in a single time segment for an entire maneuver history. Problems with data correlation and hysteresis of the heating ratio profile have been eliminated with this model. However, a time skew in this data has been verified to obtain reasonable values for the coating thickness and heating ratios. This supports the theory of the nonisothermal wall effect on the OMS pod.

Lower surface data from both STS-2 and STS-4 has been processed with the new algorithm. Nonlinear heating models applied to the STS-2 data verify the linear heating rate assumption on the lower surface. Estimation of initial conditions of the STS-4 Mach 12 Pushover Pullup maneuver has provided a more accurate estimation of parameters. Values for the heating ratio are close for the laminar flow STS-2 Mach 20 and STS-4 Mach 12 maneuvers as compared with the turbulent STS-4 Mach 8 case. However, the heating derivative of the STS-4 Mach 12 maneuver remains low compared to that of the STS-2 Mach 20 case and indicates the presence of an unmodeled Mach or Reynolds number effect.

## 6.2 Recommendations

The flexibility of the new heating model may be enhanced by improving the ability to estimate the knots of the multiple

segment model. One possibility may be to store sensitivities for each linear segment individually as they are calculated. As the model changes from one segment to another, these stored values, rather than zero values, may be used as starting points for the propagation of the sensitivities.

Additional modifications to the algorithm may include placing an upper bound on the coating thickness estimate. This would provide better parameter estimates in the presence of the nonisothermal wall and would aid in determining the necessary time skew. Also, direct incorporation of the non-isothermal wall effect into the scheme is desirable.

For the initial condition smoother, the use of the RC time constant approximation for the smoothing interval may be further verified by calculation of the system's eigenvalues. A better smoothing interval may be obtained from this, but added computational burden may not warrant it.

Application of this model to other nonlinear areas can be accomplished. In cases where a transient other than angle of attack is considered, minor modifications may be made to use this model in terms of the desired variable. Such an application can be made to elevon and body flap maneuvers.

Previous results obtained through the use of the linear perturbation model may be verified using the enhanced model. Lower predictions for the coating thickness may be found on areas with nonlinear heating rates. Additionally, the improved

model will provide better estimates of the heating ratio for these areas.

The Mach or Reynolds number effect found on STS-4 should be investigated more thoroughly. Applying Mach or Reynolds number perturbations in the nonlinear form described for angle of attack in this paper may provide greater insight into a little understood phenomenon.

Another important area for use of this model is in transient heat transfer measurements made in the wind tunnel. The HEATEST program has been used to analyze data for such a technique (Ref 11). In this technique, only one transient is considered (angle of attack) and thus lends itself to analysis using this model. Simulations of nonlinear heating rates may be conducted in the wind tunnel, with subsequent analysis using the HEATEST program. This technique will aid greatly in the understanding of the flow phenomena on the Space Shuttle Orbiter itself.

### 6.3 Summary

As the data reduction of the Space Shuttle flight test program progresses, the enhanced HEATEST program should provide AFFTC and NASA with a more powerful analytical tool. In addition to the recommendations given here, there exists a myriad of possible applications for the new scheme. Complete knowledge of the reentry aerothermodynamic environment is necessary for landing profiles to Vandenberg AFB and elsewhere.

Thorough testing and analyses of all available data using the improved program should provide the means for safe aerothermo-dynamic envelope expansion for the Space Shuttle Orbiter.

## BIBLIOGRAPHY

1. Audley, D.R. and Hodge, J.K. "Identifying the Aero-thermodynamic Environment of the Space Shuttle Orbiter, Columbia." 6th IFAC Symposium on Identification and System Parameter Estimation, June 1982.
2. Beck, J.V. and Arnold, K.J. Parameter Estimation in Engineering and Science. John Wiley, 1977.
3. Davis, P.J. Interpolation and Approximation. Blaisdell, 1963.
4. Ewing, R.E. "The Approximation of Certain Parabolic Equations Backward in Time by the Sobolev Equations," SIAM Journal of Math. Anal., Vol. 6, pp. 283-294, April, 1975.
5. Eykhoff, Pieter. System Identification. John Wiley, 1974.
6. Fraser, D.C., and Potter, J.E. "The Optimum Linear Smoother as a Combination of Two Optimum Linear Filters," IEEE Trans. Automat. Control. Vol. 7, pp. 387-390, 1969.
7. Hodge, J.K. "Trends in Shuttle Entry Heating from the Correlation of Flight Test Maneuvers," NASA Langley Conference on Shuttle Performance: Lessons Learned, March, 1983. To be published as NASA CP.
8. Hodge, J.K. and Audley, D.R. "Aerothermodynamic Parameter Estimation from Space Shuttle Thermocouple Data during Transient Flight Test Maneuvers," AIAA-83-0482, January, 1983.
9. Hodge, J.K., Audley, D.R., Phillips, P.W., and Hertzler, E.K. "Aerothermodynamic Flight Envelope Expansion for a Manned Lifting Reentry Vehicle (Space Shuttle)." Paper 3-B, AGARD CP-339, October, 1982.
10. Hodge, J.K., Phillips, P.W., and Audley, D.R. "Flight Testing a Manned Lifting Reentry Vehicle (Space Shuttle) for Aerothermodynamic Performance." AIAA-81-2421, November, 1981.
11. Hodge, J.K., Woo, Y.K., and Cappelano, P.T. "Parameter Estimation for Imbedded Thermocouples in Space Shuttle Wind Tunnel Test Articles with a Nonisothermal Wall," AIAA-83-1533, June, 1983.

12. Jazwinski, A.H. Stochastic Processes and Filtering Theory. Academic Press, 1970.
13. Kaplan, M.H. Space Shuttle: America's Wings to the Future. Aero Publishers, 1978.
14. Lattes, R., and Lion, J.L. The Method of Quasireversibility, Applications to Partial Differential Equations. American Elsevier, 1969
15. Maybeck, P.S. Stochastic Models, Estimation, and Control, Vols. I and II, Academic Press, 1979 (Vol. I) and 1982 (Vol. II).
16. Meditch, J.S. Stochastic Optimal Linear Estimation and Control. McGraw-Hill, 1969.
17. Payne, L.E. Improperly Posed Problems in Partial Differential Equations. Society for Industrial and Applied Mathematics, 1975.
18. Prenter, P.M. Splines and Variational Methods, John Wiley, 1975.
19. Rao, C.R. Advanced Statistical Methods in Biometric Research. Chapter 4, John Wiley, 1952.
20. Sagstetter, P.W. "Numerical Computation of the Matrix Riccati Equation for Heat Propagation During Space Shuttle Reentry," M.S. Thesis, AFIT/GCS/MA/82D-7, Air Force Institute of Technology, Wright Patterson AFB, Ohio, 1982.
21. Showalter, R., and Ting, T.W. "Pseudo-Parabolic Partial Differential Equations," SIAM Journal Math. Anal., Vol. 1, pp. 1-26, 1970.
22. Space Shuttle Orbiter Entry Aerodynamic Heating Data Book. Rockwell International Space Division, Document Number SD73-SH-0184 C Revision, Books 1 and 2, October, 1978.
23. Walter, W. "On Existence and Nonexistence in the Large of Solutions of Parabolic Differential Equations with a Nonlinear Boundary Condition," SIAM Journal Math. Anal., Vol. 6, pp. 85-90, 1975.

24. Williams, S.D., and Curry, D.M. "An Analytical and Experimental Study Using a Single Embedded Thermocouple," Journal of Spacecraft and Rockets, Vol. 14, pp. 632-637, October, 1977.  
(see also "Technical Comments," Journal of Spacecraft and Rockets, Vol. 15, pp. 381-383, November, 1978).

## Appendix A

### Piecewise Linear Interpolation

This section describes the piecewise linear interpolation model for the heating ratio mentioned in Section 2.3. The development of this model draws from approximation and interpolation theory, details of which are given by Davis and Prenter (Refs 3,18).

For simplicity in development, it will be assumed that the heating ratio is a function only of angle of attack,  $f(\alpha)$ . It will also be assumed that this function is unknown for a given maneuver and in general is not adequately described by the linear perturbation form originally derived for the HEATEST algorithm. The problem then becomes one of finding a suitable description for this model to be used in the estimation setting of the identification process. The solution process is thus unique in that it seeks to estimate an approximating function for the heating ratio.

If the heating ratio,  $f(\alpha)$ , can be described on the interval  $(a,b)$ , then this interval may be partitioned into a finite number of subintervals described by  $a = \alpha_0 < \alpha_1 < \alpha_2 < \dots < \alpha_n = b$ . These numbers,  $\alpha_0, \dots, \alpha_n$ , are called "knots" in spline theory (Ref 18) and represent points at which the behavior of the approximating function,  $\tilde{f}(\alpha)$ , is

constrained. Specifically, the approximating function will interpolate the heating ratio at these knots by  $\tilde{f}(\alpha_i) = f(\alpha_i)$  for each  $i = 0, 1, 2, \dots, n$ . Davis (Ref 3) described the Lagrange polynomials as among the simplest and most practical of interpolating polynomials. One effective way of approximation is to piece together Lagrange polynomials of a fixed degree and force them to interpolate the given data (Ref 18). The resulting function,  $s(\alpha)$ , is known as a piecewise Lagrange polynomial of degree  $m$ :

$$a_0 + a_1\alpha + \dots + a_m\alpha^m \quad \alpha_0 \leq \alpha \leq \alpha_m$$

$$s(\alpha) = a_{m+1} + a_{m+2}\alpha + \dots + a_{2m+1}\alpha^m \quad \alpha_m \leq \alpha \leq \alpha_{2m+1}$$

$$a_{2m+2}\alpha + a_{2m+3}\alpha^m + \dots + a_{3m+2}\alpha^m \quad \alpha_{2m} \leq \alpha \leq \alpha_{3n}$$

.

.

.

where the  $a_i$ 's are constants determined by  $s(\alpha_i) = f(\alpha_i)$ ,  $i = 0, 1, \dots, n$ , and  $n$  is some multiple of  $m$ .

Prenter (Ref 18) indicates that an effective approximation may be made by choosing  $m=1$  such that the function becomes piecewise linear

$$\begin{aligned}
 & a_0 + a_1 \alpha & \alpha_0 \leq \alpha \leq \alpha_1 \\
 S(\alpha) = & a_2 + a_3 \alpha & \alpha_1 \leq \alpha \leq \alpha_2 \\
 & a_4 + a_5 \alpha & \alpha_2 \leq \alpha \leq \alpha_3 \\
 & \vdots & \\
 & \vdots &
 \end{aligned} \tag{A-1}$$

where the  $a_i$ 's represent slopes for each line segment and may be replaced by a descriptive form,  $q_{\alpha i}$ . For the purpose at hand, such a function is advantageous in that it eliminates the additional computational burden of higher order polynomials. In addition, it retains a form similar to the original linear perturbation approximation and thus is easily implemented. A different form of equation (A-1) may be written by defining a step function,  $\delta_i(\alpha)$ , such that

$$\begin{aligned}
 \tilde{f}(\alpha) = & q_0 + q_{\alpha 1}(\delta_1(\alpha) - \alpha_0) + q_{\alpha 2}(\delta_2(\alpha) - \alpha_1) \\
 & + \dots + q_{\alpha n}(\delta_n(\alpha) - \alpha_{n-1})
 \end{aligned} \tag{A-2}$$

where

$$\begin{aligned}
 \delta_i(\alpha) = & \alpha & \alpha_{i-1} \leq \alpha \leq \alpha_i \\
 & \alpha_i & \alpha \leq \alpha_i
 \end{aligned}$$

The step function,  $\delta_i(\alpha)$ , represents the discontinuous

nature of the model at the knot,  $\alpha_i$ ,

In general, the unknown parameters in this model formulation are the intercept,  $q_o$ , the slopes,  $q_{\alpha i}$ , and the knots,  $\alpha_i$ . Note that the intercept,  $q_o$ , is the same as that given in (2-4). Often it may be desirable to specify the location of the knots and thus constrain the approximation to interpolate more precisely near a given angle of attack. However, a better fit of the heating ratio throughout the range of angles of attack would occur when the location of these knots is determined by the estimation scheme itself.

To estimate these parameters by the method of Chapter III, it is necessary to calculate the model sensitivity with respect to each unknown parameter. The derivative of equation (A-2) with respect to any slope,  $q_{\alpha i}$ , can be given as

$$\frac{\partial \tilde{f}(\alpha)}{\partial q_{\alpha i}} = \delta_i(\alpha) - \alpha_{i-1} \quad (A-3a)$$

By defining a different step function,  $\alpha_i(\alpha)$ , the derivative of equation (A-2) with respect to any knot,  $\alpha_i$ , may be given as

$$\frac{\partial \tilde{f}(\alpha)}{\partial \alpha_i} = \gamma_i(\alpha) - q_{\alpha i+1} \quad (A-3b)$$

$$\gamma_i(\alpha) = \begin{cases} q_{\alpha_{i+1}} & \alpha \leq \alpha_i \\ q_{\alpha_i} & \alpha > \alpha_i \end{cases}$$

The sensitivity state in general is found by solving the propagation equation given by (2-7):

$$\hat{u}_{\theta_k} = c_k \hat{u}_{\theta_k} + D_k$$

where the forcing function vector,  $D_k$ , is defined by equations (A-3). Solving this equation requires a time derivative of Equations (A-3). In general, the time derivatives of the step functions,  $\delta_i(\alpha)$  and  $\gamma_i(\alpha)$ , are undefined due to the discontinuity at the knot,  $\alpha_i$ . Thus, these step functions are approximated as constants locally in angle of attack and sensitivities are calculated for each line segment in the model. This approximation works well for calculating the slope sensitivities, but proves more tenuous for the knot sensitivities. In cases where the time rate of change of angle of attack is large in the vicinity of the knot, difficulties in estimating this parameter may be encountered.

This interpolation model was implemented into the HEATEST with the capability of estimating models up to four segments (i.e. four slopes and three knots). Application is currently limited to angle of attack modulation, but could be applied to any variable given in Equation (2-4) with minor modifications.

## Appendix B

### Backwards Heat Equation

The use of an extended Kalman filter in a backwards filter/smooth requires the solution of Equations (2-1) backward in time starting from some final condition  $t_f$ , to the initial time  $t_i$ . With the time derivative written as a first order backward difference of the form (2-2) for comparison with the original forward-running equations, the system of equations become explicit in nature in the backward scheme. An implicit form may be retained by writing the time derivative as a forward difference of the form

$$\dot{u}_i = (u_i(t_{n+1}) - u_i(t_n)) / \Delta t \quad (B-1)$$

Stability analyses show that either formulation is unstable when solved backward in time, even though the implicit scheme is unconditionally stable in the forward direction. In fact, it was determined that any conventional scheme is unsuitable. Further investigation shows this difficulty associated with solving Equations (2-2) backward in time.

Equations (2-2) are derived from the classic parabolic partial differential equation describing heat diffusion

$$u_t = u_{xx} \quad (B-2)$$

where  $u_t$  represents time differentiation and  $u_{xx}$  represents

the second partial derivative in the spatial direction. Payne identifies the "backward heat equation" as one that is improperly posed in the sense of Hadamard (Ref 17); i.e., a compatibility condition is violated and no global solution can exist. More specifically, the temperature profile at a given point in time will not depend continuously on the data and as such will have no unique solution.

Despite the improper posedness of the backward heat equation, attempts have been made to solve it, either directly or approximately. Lattes and Lions (Ref 14) present the method of "quasireversibility" which has many of the same features as the method of artificial viscosity used in solving fluid and gas dynamic problems. In this method, the partial derivative operator is perturbed in order to stabilize the problem and the limiting behavior is investigated as the perturbation vanishes. A variation of the quasireversibility method is the "pseudoparabolic" method of Showalter (Ref 21), in which an alternative perturbation form is given. These techniques are largely analytic and are not suitable for solution of the problem at hand.

Ewing (Ref 4) presents numerical results based on Showalter's method. The backward heat equation is cast in a Hilbert space setting and is approximated by the pseudoparabolic or Sobolev equation. A Crank-Nicolson method is used to solve the Sobolev equation numerically with mixed results.

Ewing states that it would be "overly optimistic" to expect good results all the way back to the initial time. This alone makes this method infeasible as an initial condition smoother.

Finally, none of these methods apply to the case of the heat equation with the nonlinear boundary condition, although Walter (Ref 23) mentions this case in an abstract setting. Thus, the difficulties associated with solving the problem at hand in a backward filter context prove enormous and the alternative method of using the linearized form of the state transition matrix in a fixed-point smoother becomes desirable.

APPENDIX C

Heating Model Simulation Results

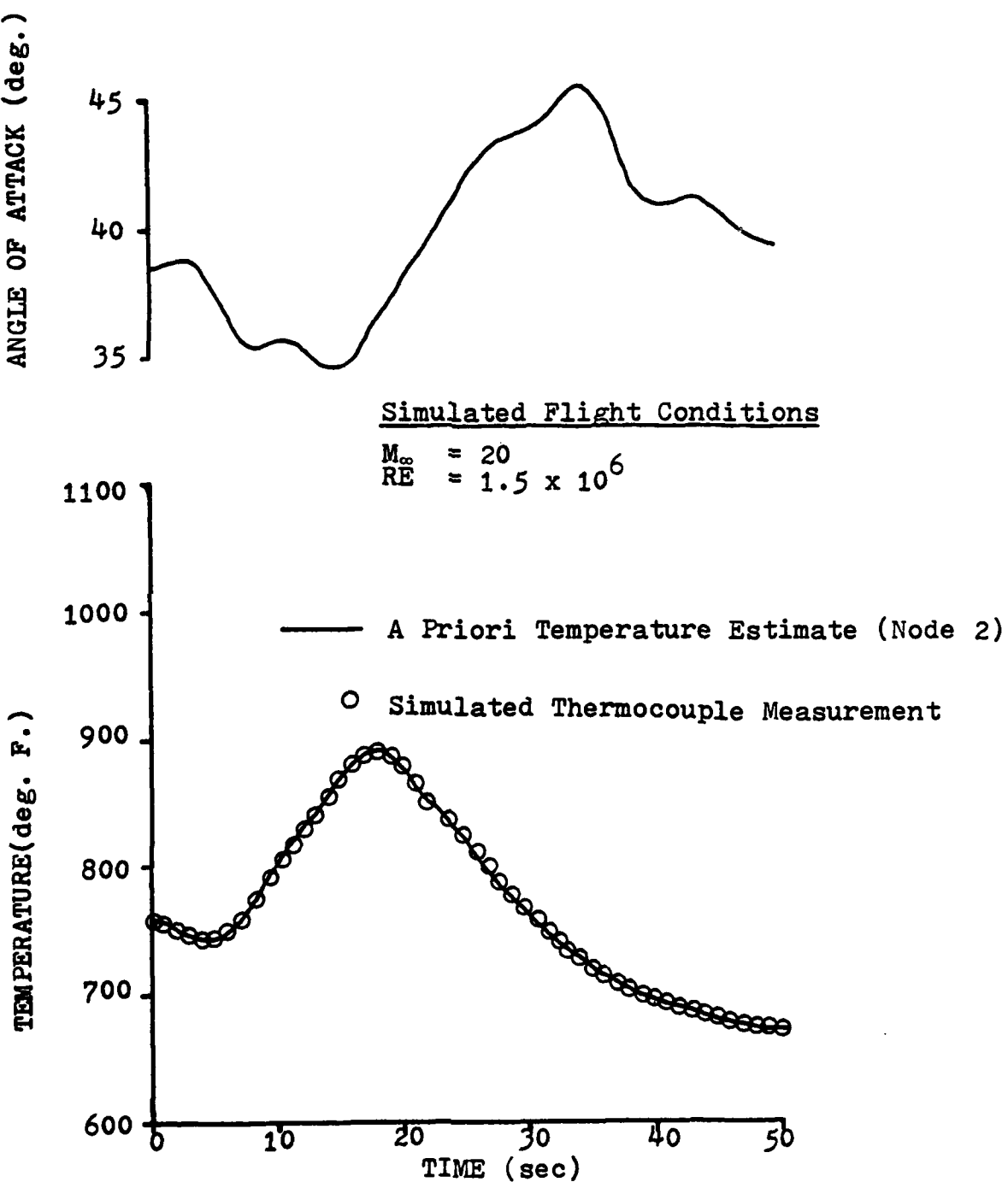


Figure C.1. Simulated Thermocouple Data (Two Segment Model)

TABLE C-1 Estimates for a Two Segment Model Simulation

<u>Parameter</u>	<u>Specified Value</u>	<u>Estimated Value (Cramer-Rao Bound)</u>
$\Delta x_A$	.00125	.00125 ( $\pm$ .00015)
$q_{\alpha_0}$	.05500	.05494 ( $\pm$ .00360)
$q_{\alpha_1}$	-.00490	-.00488 ( $\pm$ .00025)
$q_{\alpha_2}$	-.00040	-.00040 ( $\pm$ .00025)
$a_1$	39.200	39.220 ( $\pm$ .3400)

$\alpha_0 = 30$  degrees

Average Error = 0.49437

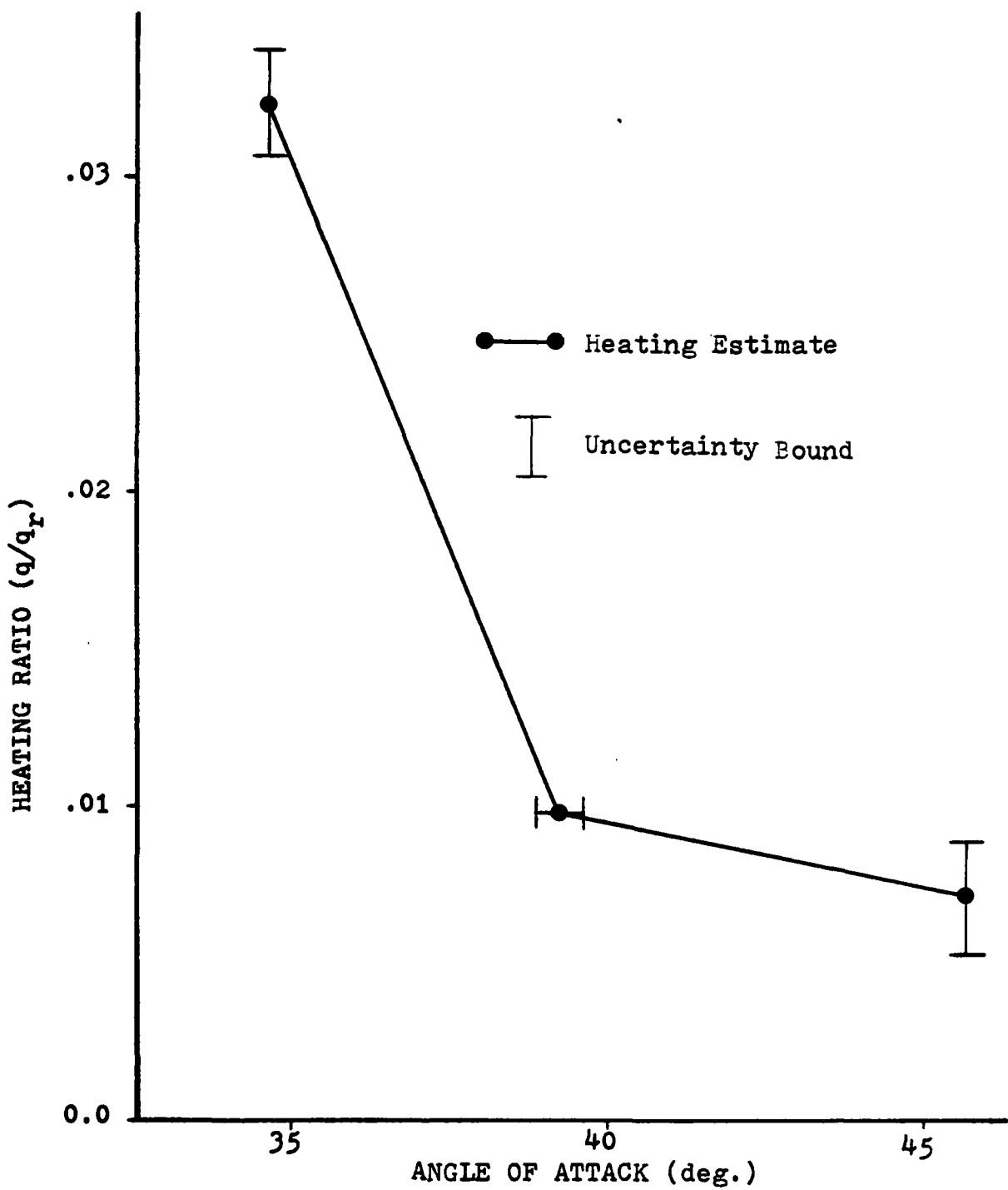


Figure C.2. Simulated Two Segment Heating Model

TABLE C-2 Estimates for a Three Segment Model Simulation

A. Estimated Coating Thickness

<u>Parameter</u>	<u>Specified</u>	<u>1 Segment (C-R Bound)</u>	<u>2 Segments (C-R Bound)</u>	<u>3 Segments (C-R Bound)</u>
$\Delta x_A$	.00125	.00157 $(\pm .00024)$	.00125 $(\pm .00018)$	.00125 $(\pm .00020)$
$q_0$	.0550	.03781 $(\pm .0021)$	.05227 $(\pm .0045)$	.0550 $(\pm .0071)$
$q_{a_1}$	-.00490	-.00213 $(\pm .00021)$	-.00441 $(\pm .00070)$	-.00490 $(\pm .00120)$
$q_{a_2}$	-.0010	-	-.00052 $(\pm .00025)$	-.00100 $(\pm .00011)$
$q_{a_3}$	-.00040	-	-	-.00040 $(\pm .00068)$
$a_1$	38.1	-	38.7245 $(\pm .60 )$	38.1000 $(\pm 1.2 )$
$a_2$	41.2	-	-	41.2000 $(\pm 1.8 )$
<b>Average Error</b>	-	.44894 E-1	.12934 E-1	.75669 E-6

B. Fixed Coating Thickness and Break Points

$q_0$	.0550	.03556 $(\pm .0011)$	.05230 $(\pm .0039)$	.05500 $(\pm .0035)$
$q_{a_1}$	-.00490	-.00110 $(\pm .0001)$	-.00441 $(\pm .00064)$	-.00490 $(\pm .00055)$
$q_{a_2}$	-.0010	-	-.00052 $(\pm .00025)$	-.00100 $(\pm .00051)$
$q_{a_3}$	-.00040	-	-	-.00040 $(\pm .00035)$
<b>Average Error</b>	-	.26013 E-1	.12805 E-1	.1284 E-8

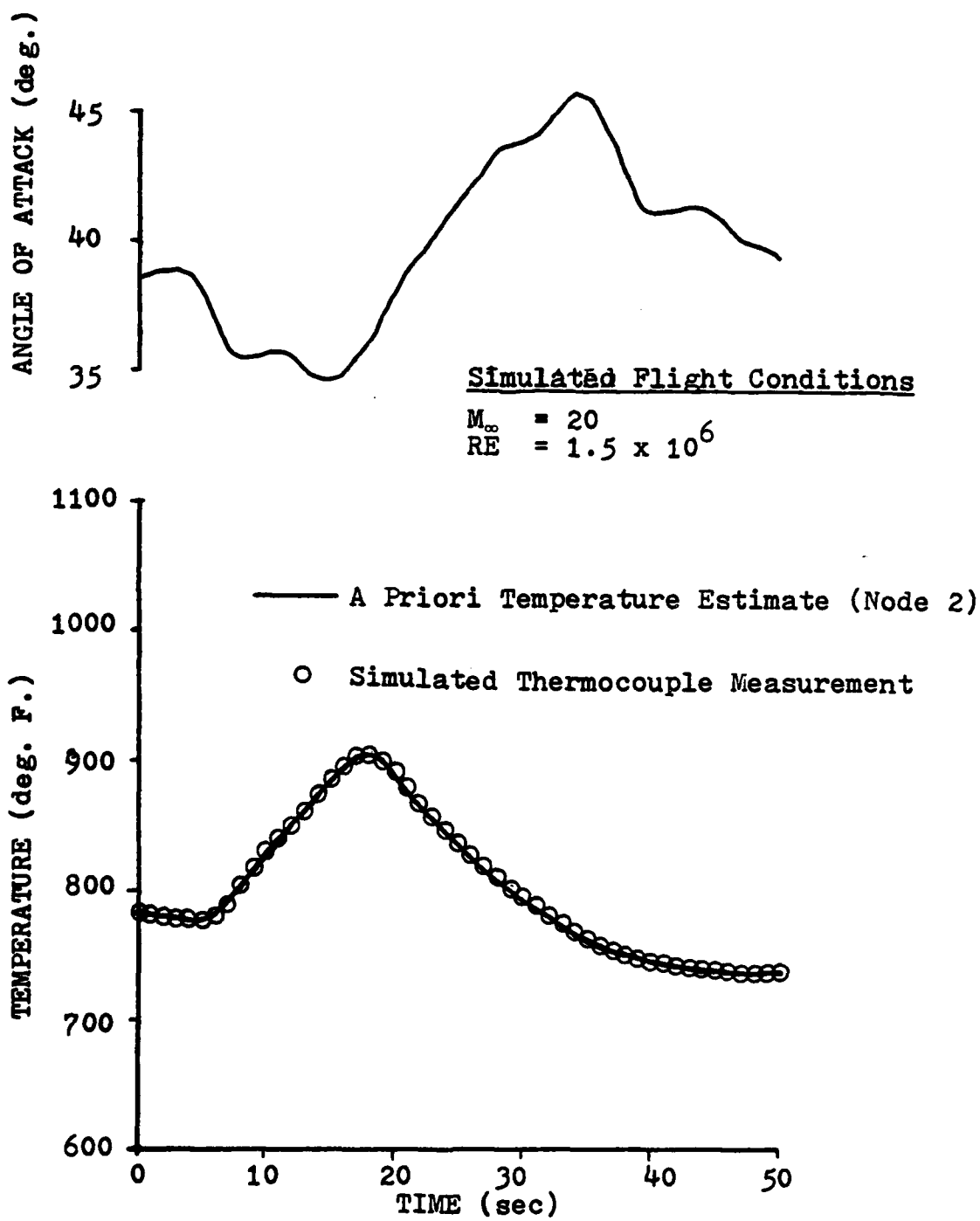


Figure C.3. Simulated Thermocouple Data (Three Segment Model)

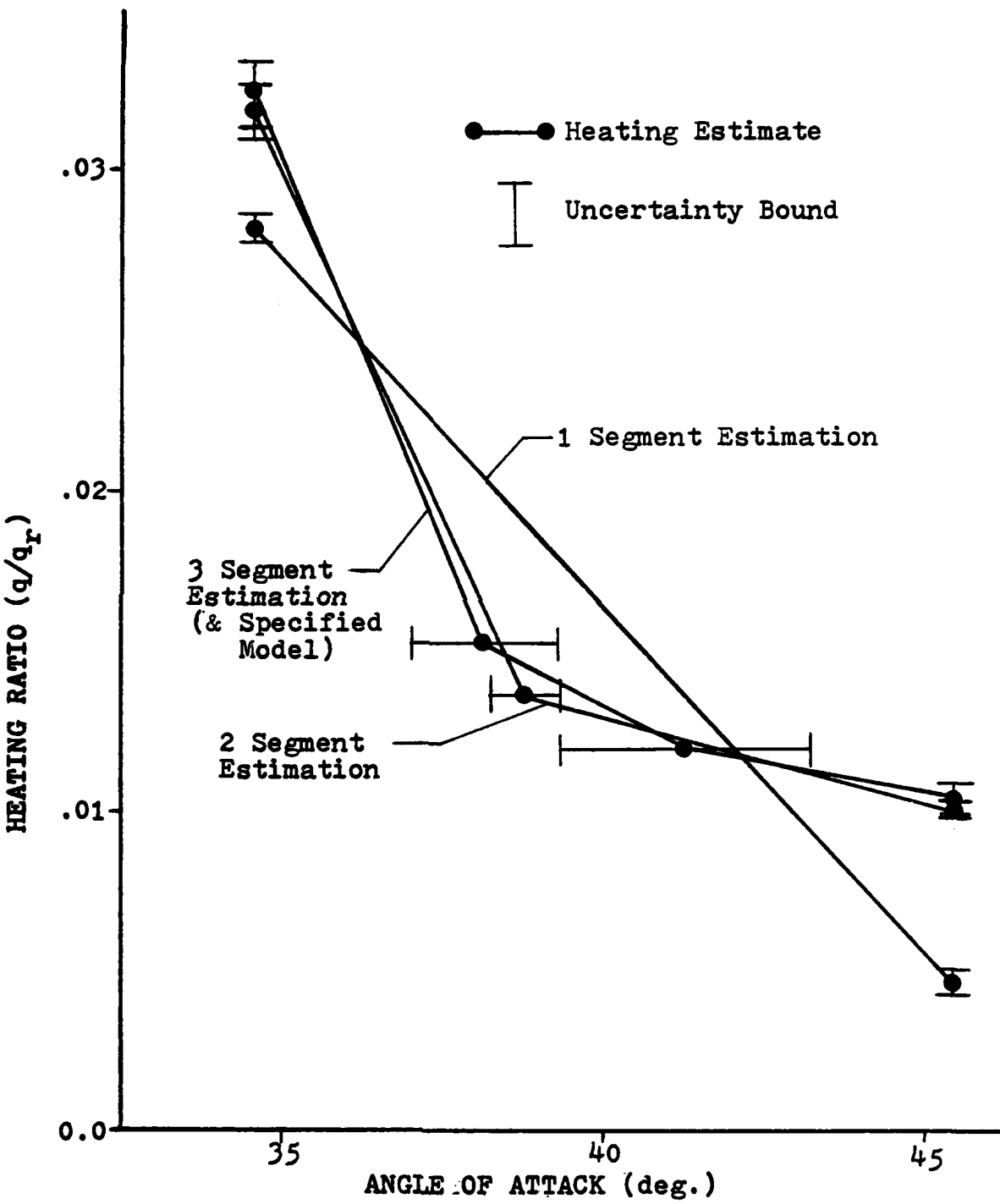


Figure C.4. Simulated Three Segment Heating Model

APPENDIX D

Heating Model Flight Data Results

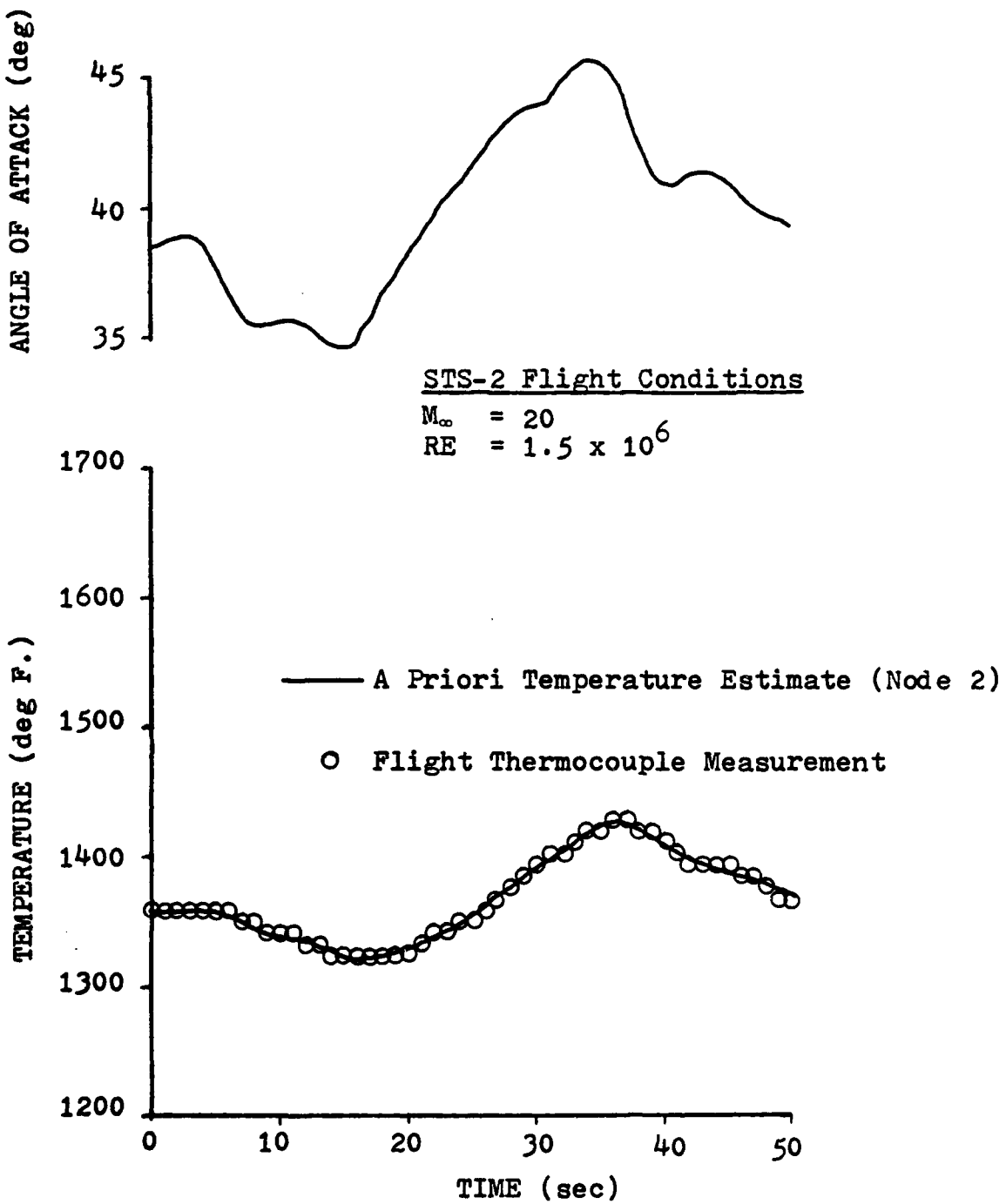
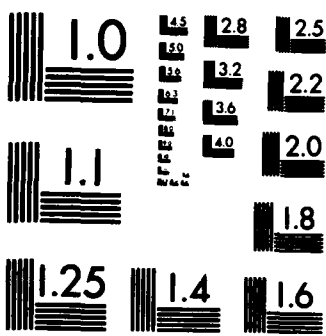


Figure D.1. Lower Surface STS-2 Flight Thermocouple Data  
(Mach 20 Pushover Pullup Maneuver)

AD-A136 928      NONLINEAR MODELING AND INITIAL CONDITION ESTIMATION FOR      2/2  
IDENTIFYING THE A. (U) AIR FORCE INST OF TECH  
WRIGHT-PATTERSON AFB OH SCHOOL OF ENGI.. C D LUTES  
UNCLASSIFIED      DEC 83 AFIT/GRE/RA/83D-14      F/G 28/13      NL

END



MICROCOPY RESOLUTION TEST CHART  
NATIONAL BUREAU OF STANDARDS-1963-A

TABLE D-1 Estimates for STS-2 Lower Surface

<u>Parameter</u>	<u>1 Segment (C-R Bound)</u>	<u>2 Segments (C-R Bound)</u>	<u>3 Segments (C-R Bound)</u>
$\Delta x_A$	.00129 ( $\pm$ .00037)	.00133 ( $\pm$ .00046)	.00136 ( $\pm$ .00047)
$q_o$	.054940 ( $\pm$ .00074)	.056510 ( $\pm$ .0057)	.05550 ( $\pm$ .0093)
$q_{\alpha_1}$	.00234 ( $\pm$ .00026)	.00183 ( $\pm$ .00080)	.00199 ( $\pm$ .00150)
$q_{\alpha_2}$	-	.00315 ( $\pm$ .00120)	.00189 ( $\pm$ .00150)
$q_{\alpha_3}$	-	-	.00333 ( $\pm$ .00120)
$\alpha_1$	-	40.47792 ( $\pm$ 1.9)	38.1 (Fixed)
$\alpha_2$	-	-	41.2 (Fixed)
Average Error	1.8028	1.2527	1.2586

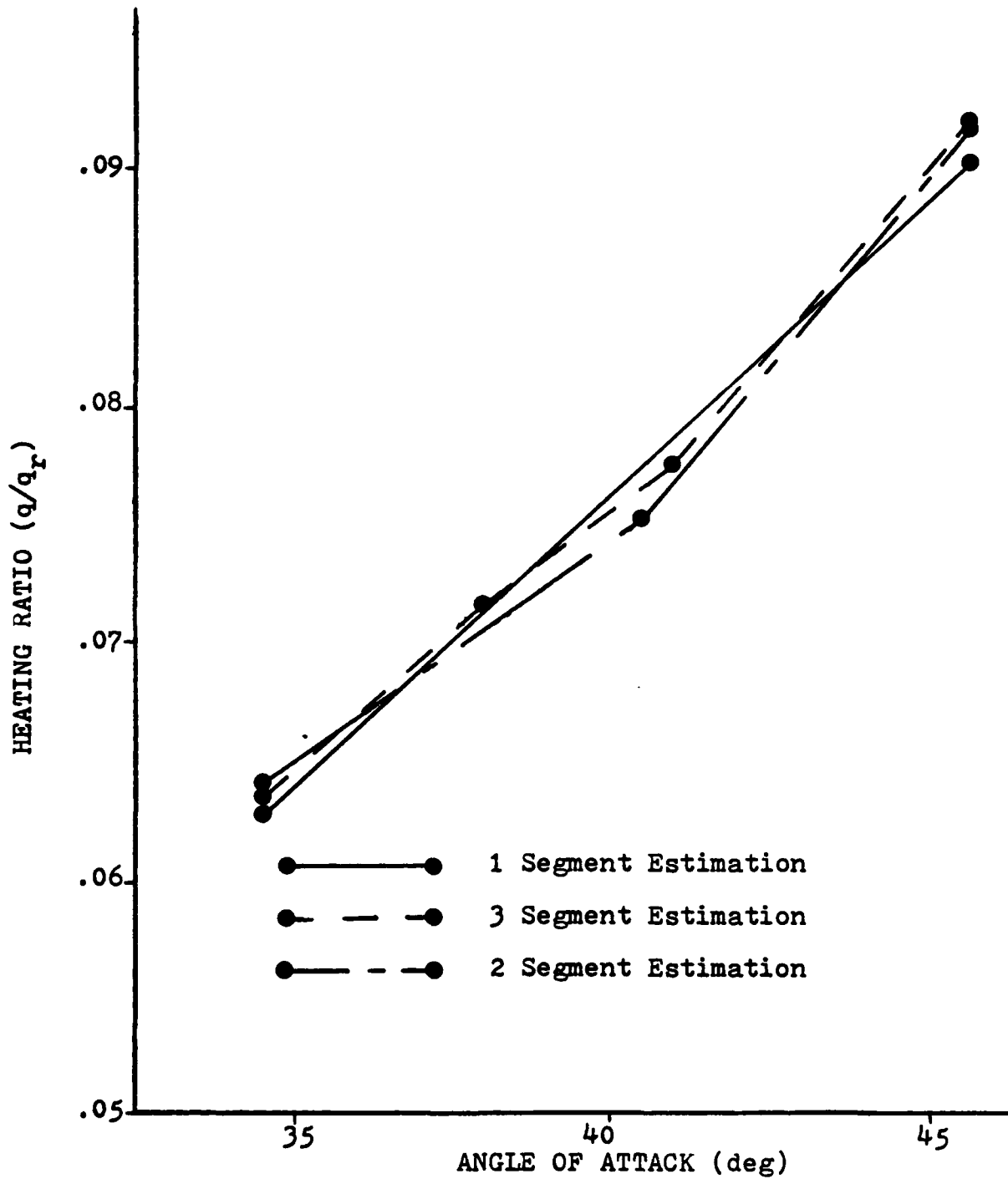


Figure D.2. STS-2 Lower Surface Heating Estimates (Mach 20 POPU)

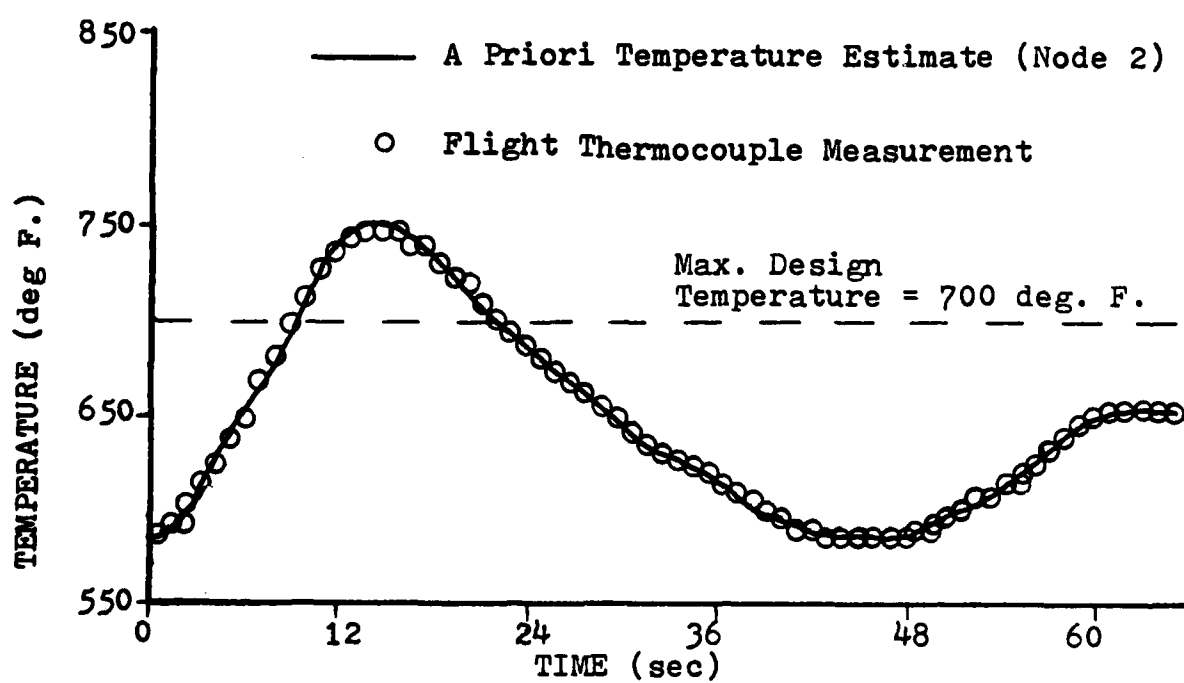
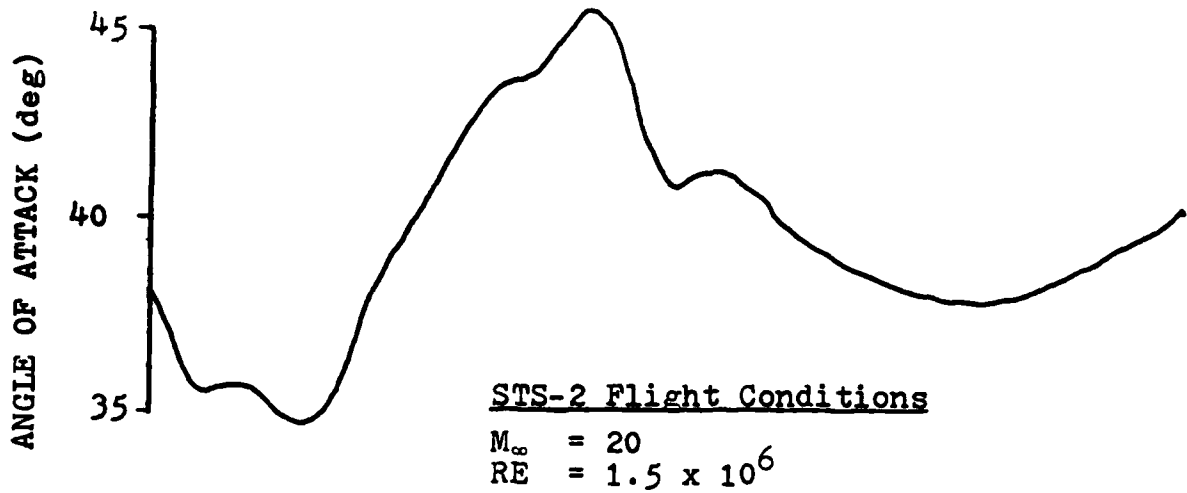


Figure D.3. OMS Pod STS-2 Flight Thermocouple Data  
(Mach 20 Pushover Pullup Maneuver)

TABLE D-2 Estimates for STS-2 OMS Pod

A. Time Segments from original HEATEST program  
 $(\alpha_0 = 40 \text{ degrees})$

	<u>Segment 1</u>	<u>Segment 2</u>	<u>Segment 3</u>	<u>Segment 4</u>
Time Range (sec)	0-16	16-29	29-49	49-60
$q_o$	.00312 ( $\pm .0057$ )	.00558 ( $\pm .0022$ )	.00621 ( $\pm .00046$ )	.00637 ( $\pm .0023$ )
$q_{\alpha}$	-.00491 ( $\pm .0013$ )	-.00040 ( $\pm .00074$ )	-.00105 ( $\pm .00036$ )	-.00307 ( $\pm .0013$ )
Average Error	.31754	.16370	.13352	.44714

B. Heating Estimates from modified program  
 $(\quad = 30 \text{ degrees})$

<u>Parameter</u>	<u>2 Segments</u>	<u>3 Segments</u>
$q_o$	.05220 ( $\pm .0037$ )	.05819 ( $\pm .0049$ )
$q_{\alpha_1}$	-.00491 ( $\pm .0005$ )	-.00601 ( $\pm .00074$ )
$q_{\alpha_2}$	-.00061 ( $\pm .00042$ )	-.00239 ( $\pm .00049$ )
$q_{\alpha_3}$	-	-.00005 ( $\pm .00006$ )
$\alpha_1$	39.3284 ( $\pm 0.48$ )	37.5 (fixed)
$\alpha_2$	-	41.5 (fixed)
Average Error	.17281	.22114

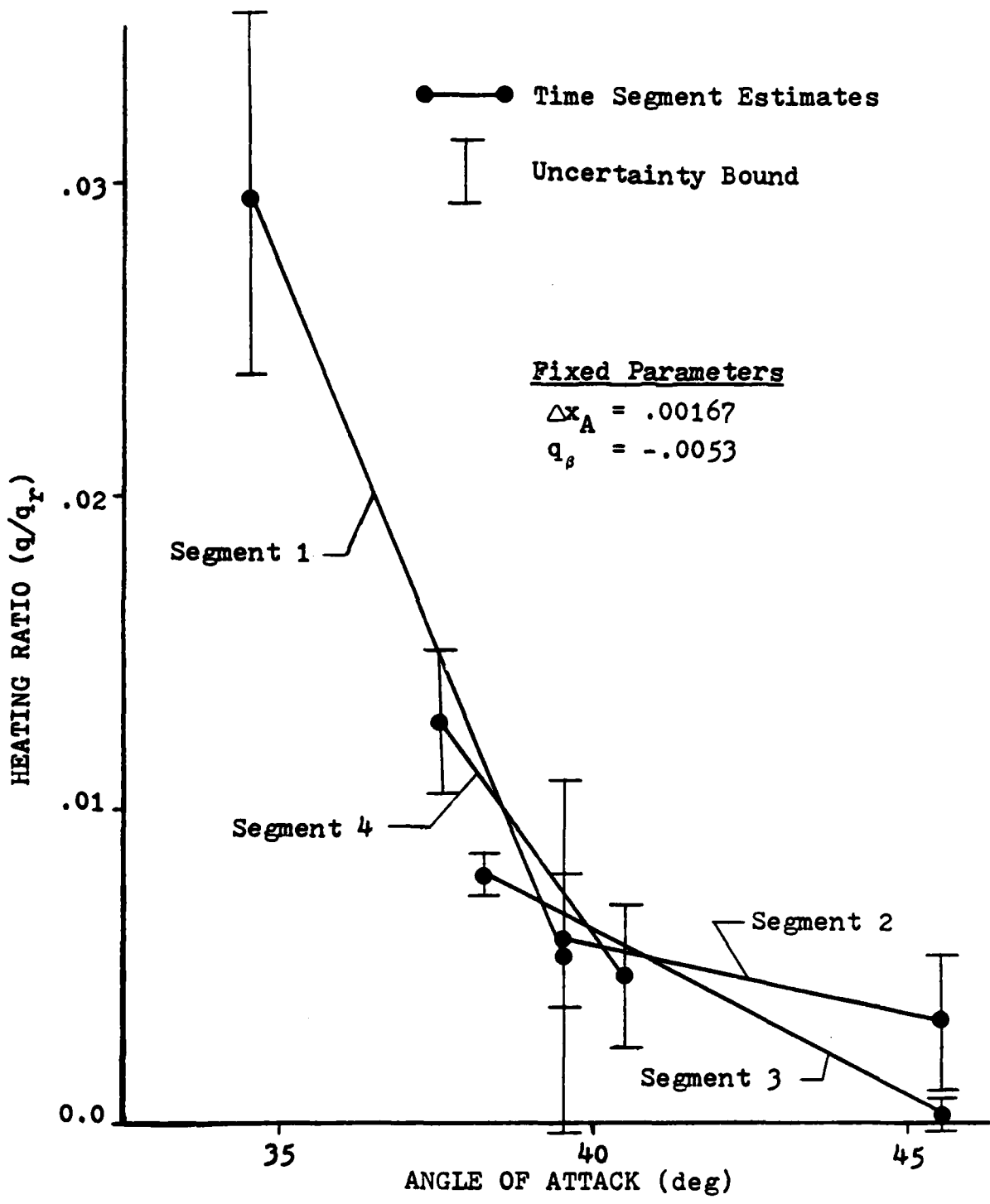


Figure D.4. Time Segment Heating Estimates for OMS Pod STS-2 Data

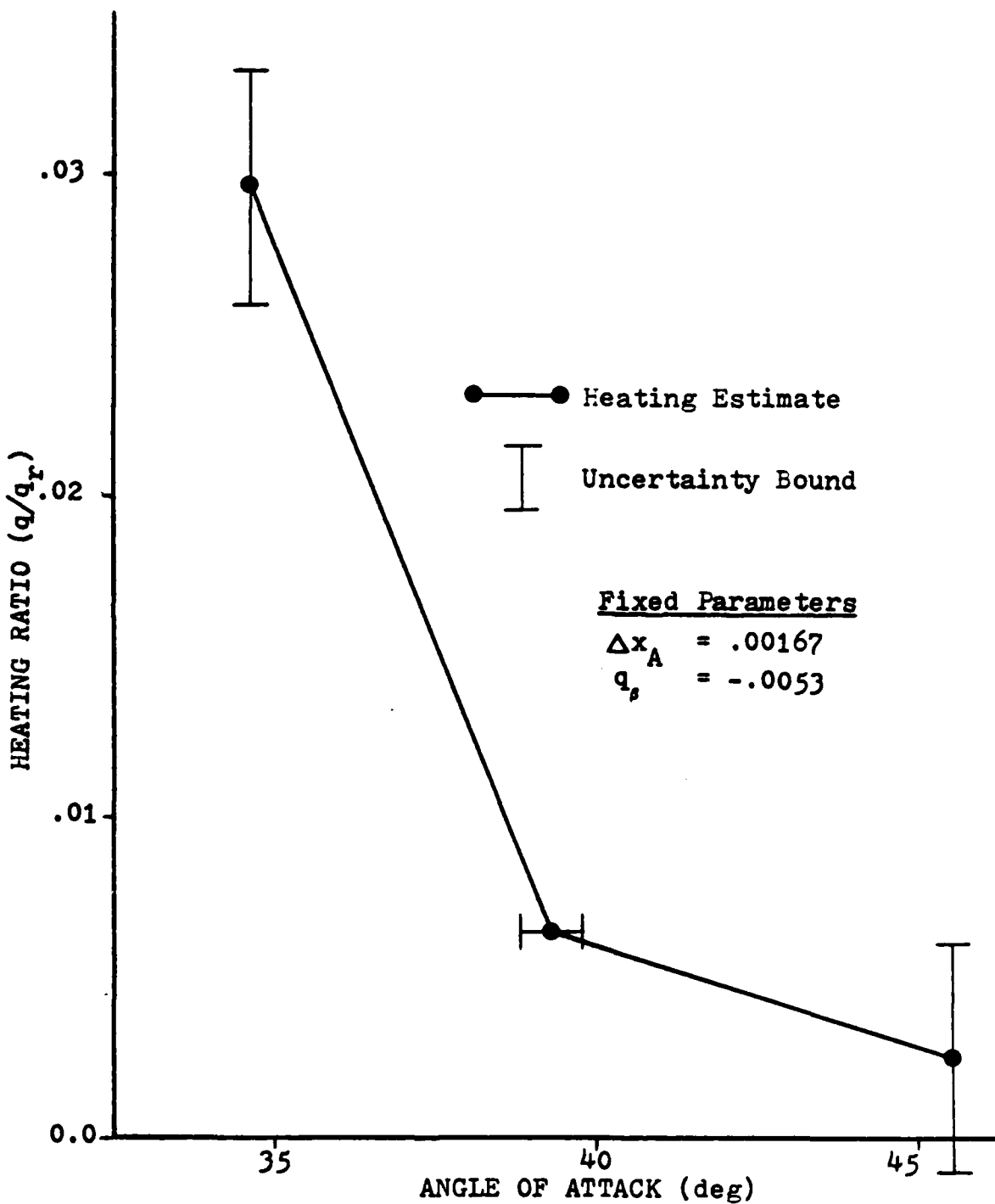


Figure D.5. Two Segment Model Heating Estimates for OMS Pod  
STS-2 Data

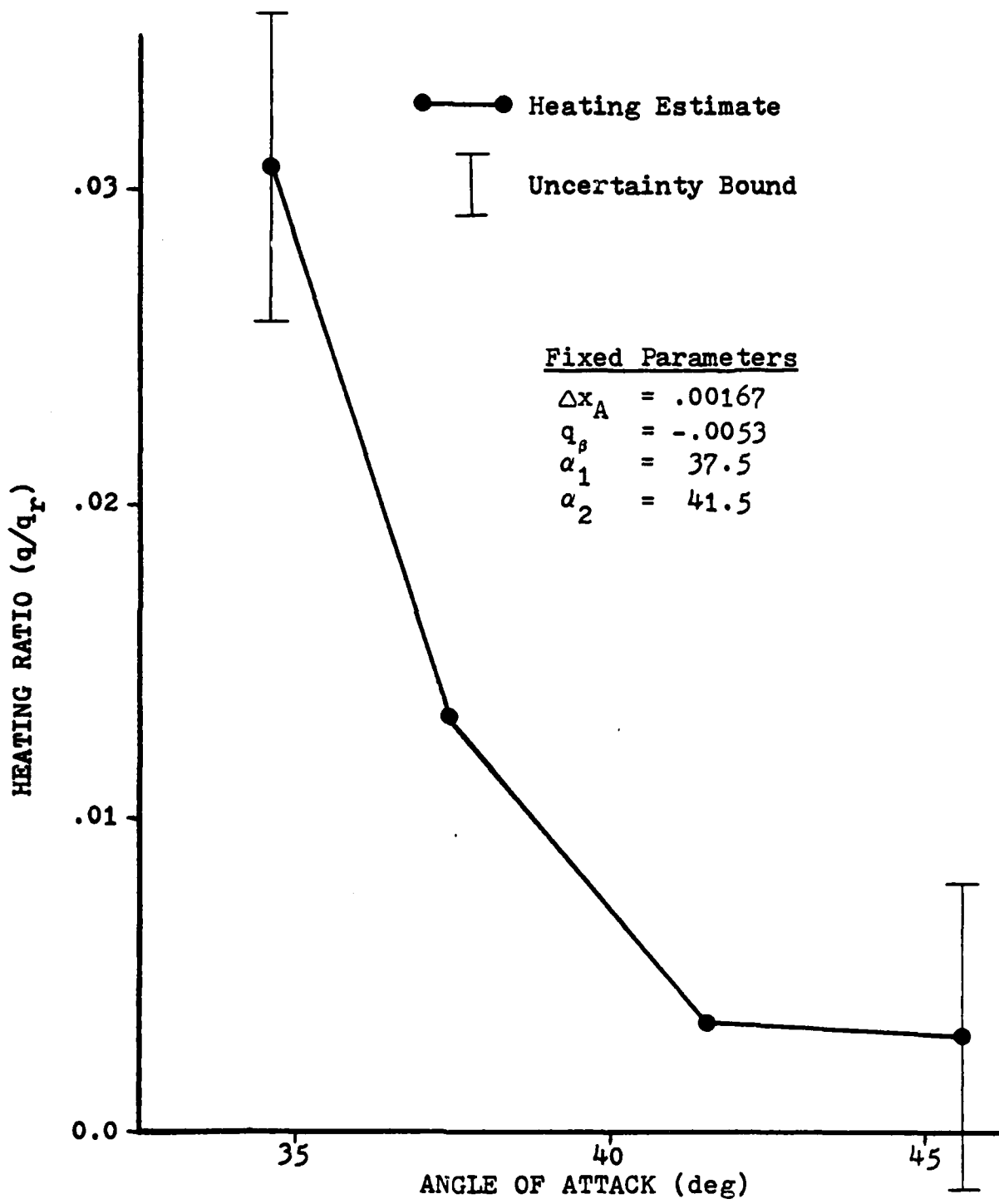


Figure D.6. Three Segment Model Heating Estimates for OMS Pod STS-2 Data

TABLE D-3 Estimates for Various Time Skews in STS-4 Data

<u>Parameter</u>	<u>No Skew</u>	<u>1 Sec</u>	<u>2 Sec</u>	<u>3 Sec</u>	<u>4 Sec</u>
$\Delta x_A$	.00349 ( $\pm .00023$ )	.00291 ( $\pm .00024$ )	.00230 ( $\pm .00023$ )	.00168 ( $\pm .00023$ )	.00118 ( $\pm .00021$ )
$q_o$	.11064 ( $\pm .0110$ )	.08900 ( $\pm .0088$ )	.07125 ( $\pm .0079$ )	.05525 ( $\pm .0069$ )	.04326 ( $\pm .0055$ )
$q_{\alpha_1}$	-.01183 ( $\pm .0015$ )	-.00923 ( $\pm .0011$ )	-.00719 ( $\pm .0010$ )	-.00533 ( $\pm .00087$ )	-.00395 ( $\pm .00069$ )
$q_{\alpha_2}$	-.00241 ( $\pm .00067$ )	-.00160 ( $\pm .00062$ )	-.00166 ( $\pm .00050$ )	-.00076 ( $\pm .00042$ )	-.00047 ( $\pm .00033$ )
$\alpha_1$	38.5398 ( $\pm .50$ )	38.8384 ( $\pm .55$ )	38.8729 ( $\pm .51$ )	38.9546 ( $\pm .55$ )	39.0269 ( $\pm .55$ )
$q_\beta$	-.01887 ( $\pm .0041$ )	-.01412 ( $\pm .0035$ )	-.01078 ( $\pm .0028$ )	-.00758 ( $\pm .0023$ )	-.00523 ( $\pm .0018$ )
Average Error	.21729	.09195	.03975	.16627	.27163

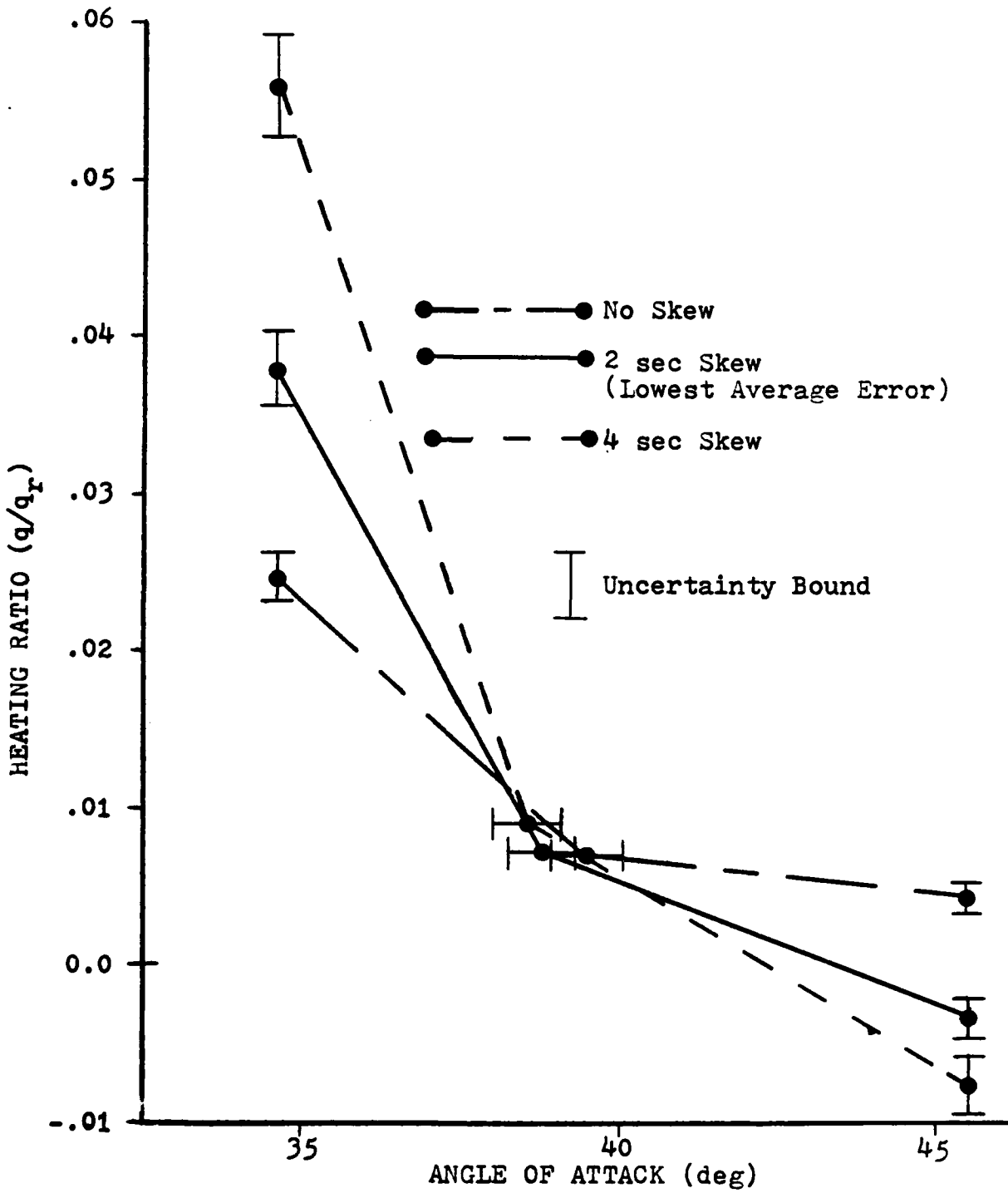


Figure D.7. Heating Estimates for Various Time Skews in OMS Pod STS-2 Data

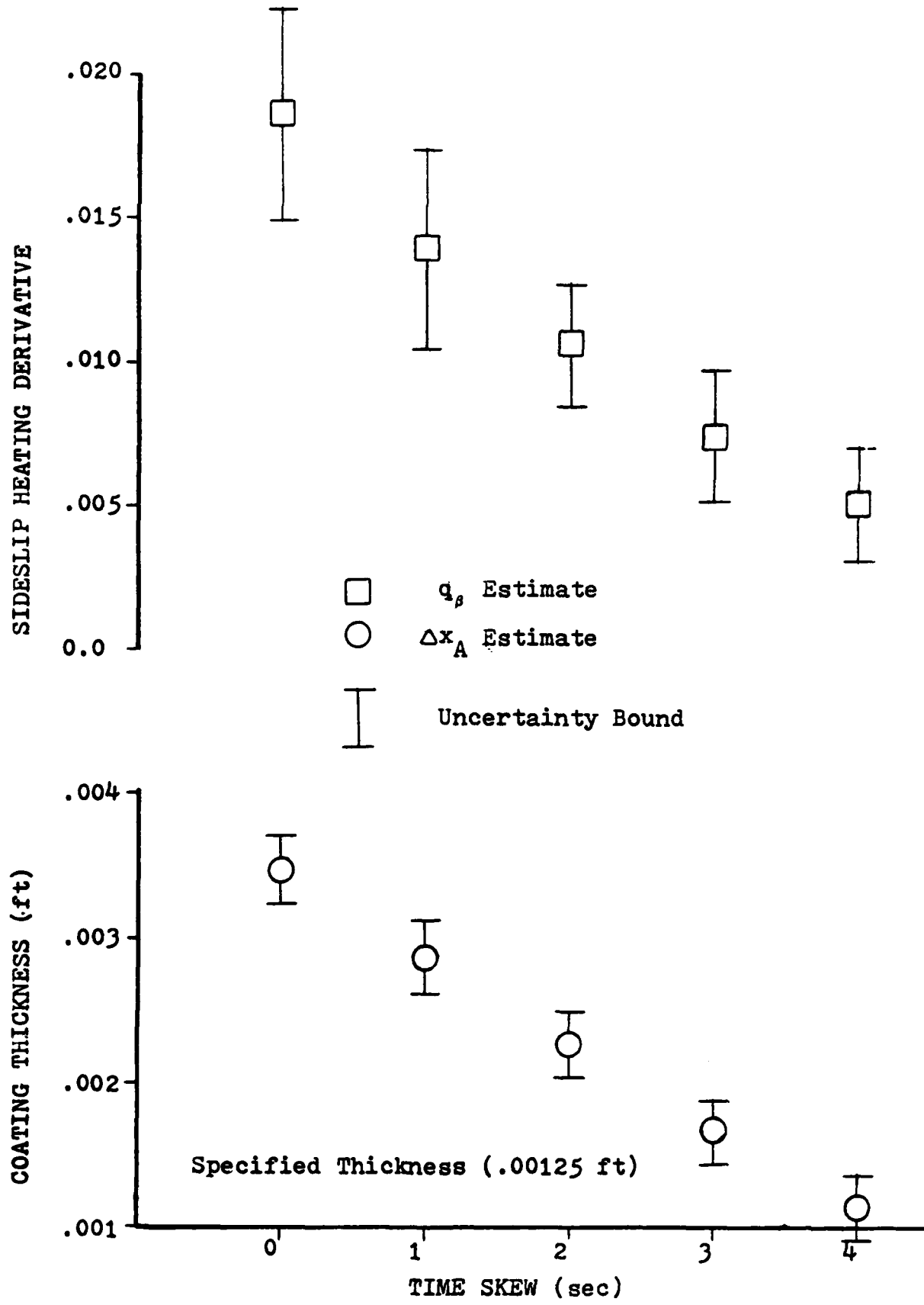


Figure D.8. Parameter Estimates for Various Time Skews in OMS Pod STS-2 Data

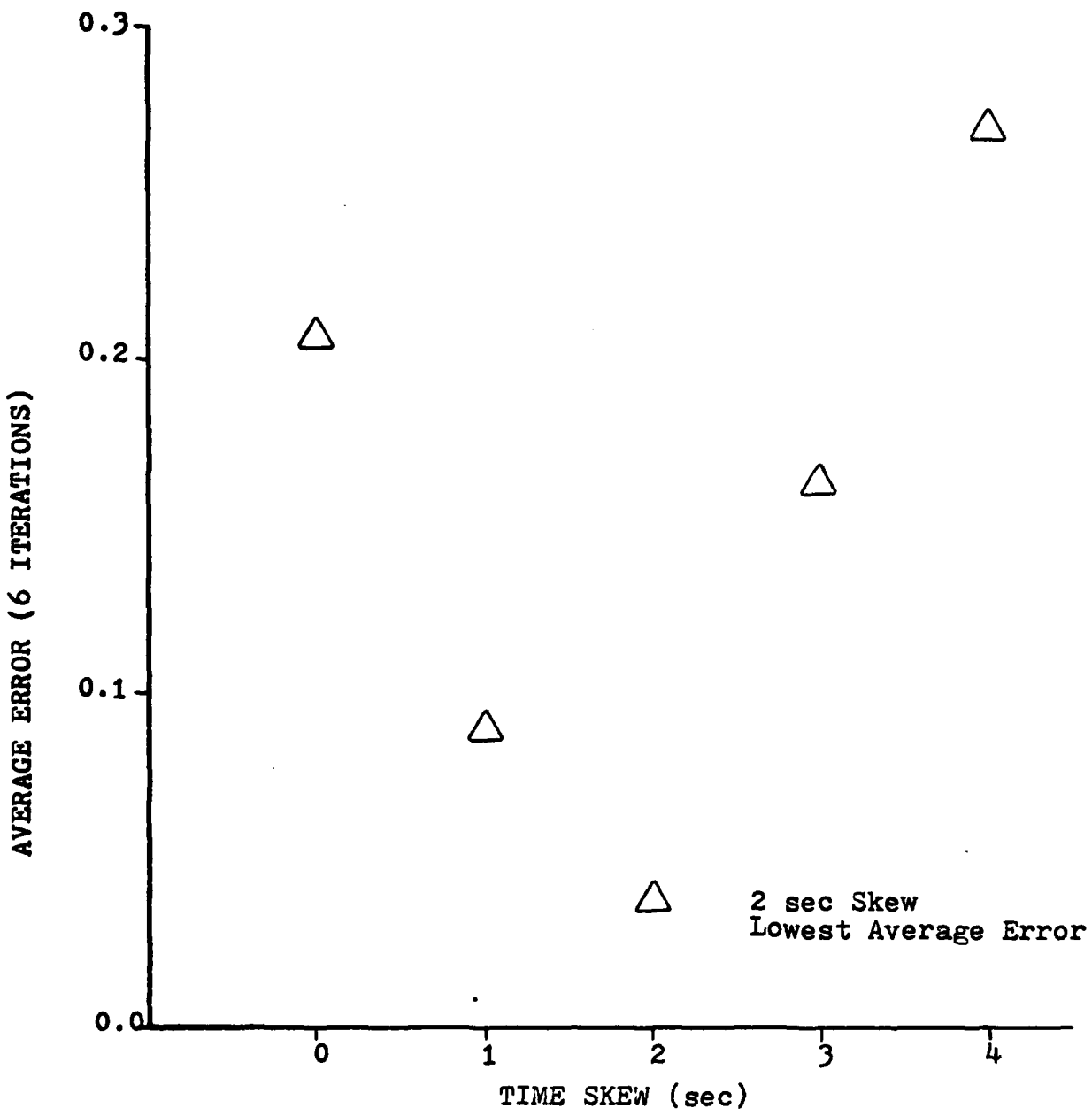


Figure D.9. Average Error of Thermocouple Nodes for OMS Pod  
STS-2 Data

APPENDIX E

Initial Condition Estimation Simulation Results

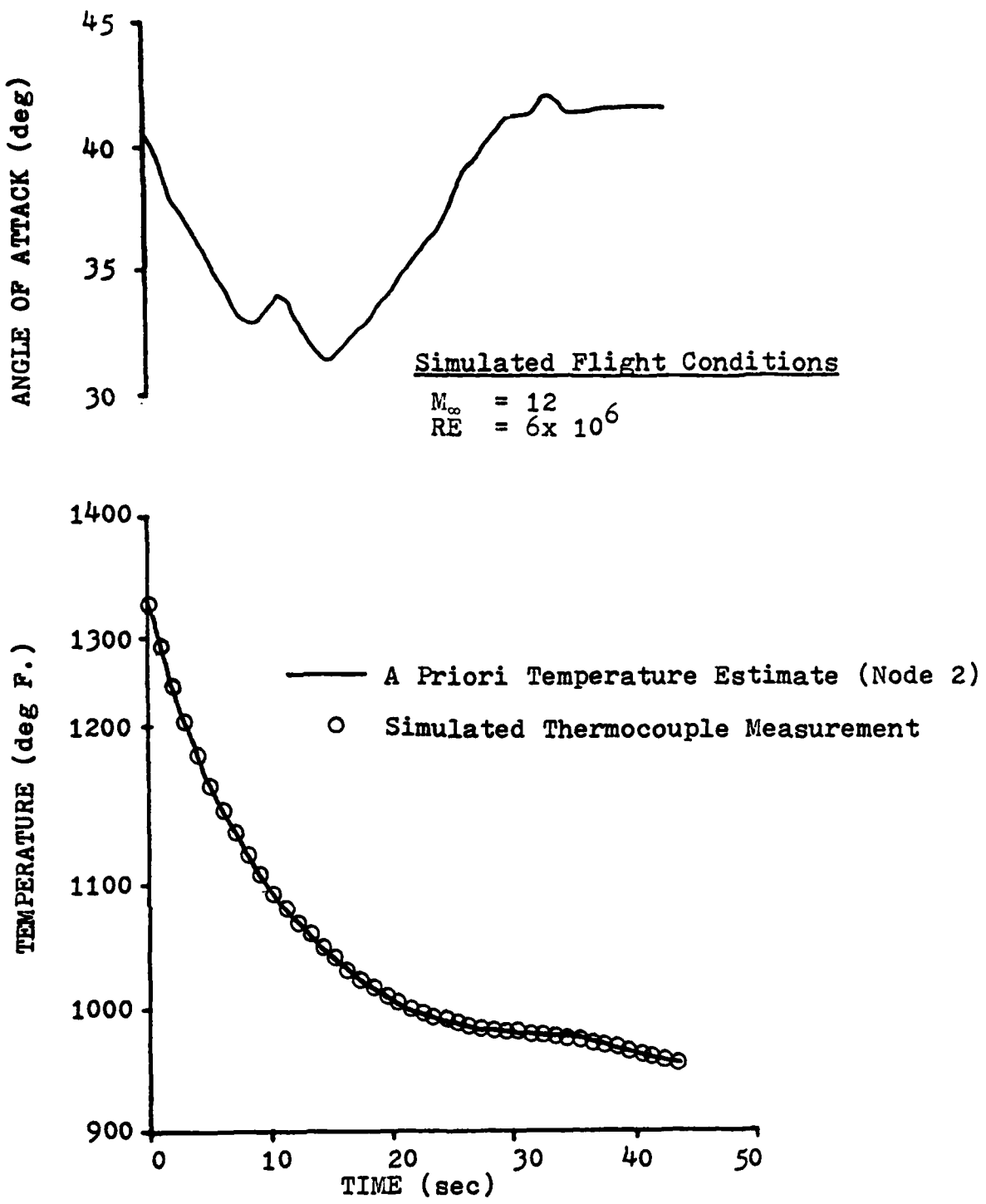


Figure E.1. Smoothing Simulation Thermocouple Data

TABLE E-1 Smoothing Simulation Results

A. Initial Condition Smoothing

<u>Node</u>	<u>Specified Initial Temp. (deg. F.)</u>	<u>Starting Initial Temp. (deg. F.)</u>	<u>Smoothed Initial Temp. (deg. F.)</u>	<u>Smoothed Initial Variance (deg. F.)</u>
1	1330	1330	1330	13.7
*2	1330	1330	1330	4.6
3	1330	1230	1328	31.0
4	1100	1017	1102	32.9
*5	1004	928	1004	3.3
6	900	832	894	29.4
7	800	772	808	24.4
*8	720	665	720	2.3
9	650	600	644	25.1
10	550	509	548	17.9
*11	499	460	499	1.3
12	122	112	122	1.7
*13	112	122	122	0.5

\* Thermocouple Node

B. Model Estimation with Smoothed Initial Conditions

<u>Parameter</u>	<u>Specified</u>	<u>Estimated</u>
$\Delta x_A$	.00125	.00125 ( $\pm .00015$ )
$q_o$	.0535	.05352 ( $\pm .0011$ )
$q_{a_1}$	.00110	.00110 ( $\pm .00024$ )

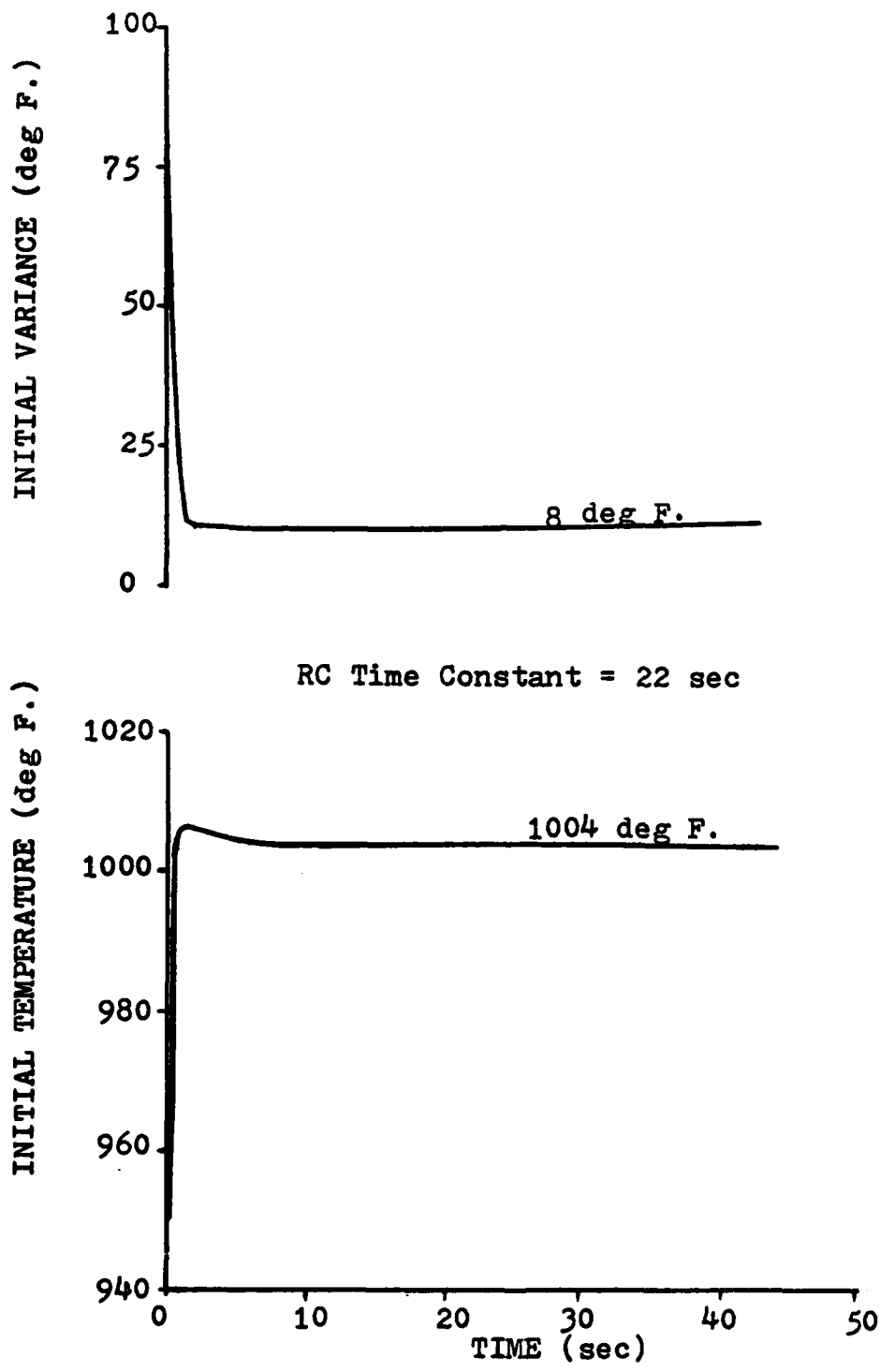
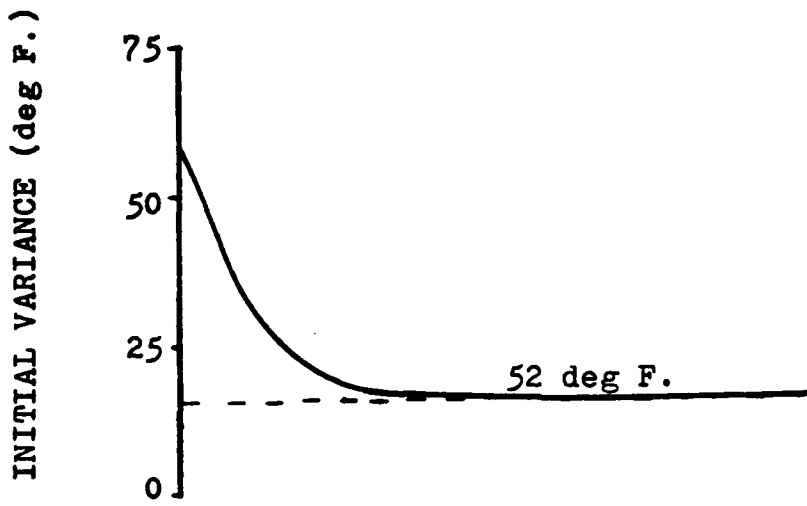


Figure E.2. Initial Condition Smoothing for a Thermocouple Node Point (Node 5)



RC Time Constant = 10 sec

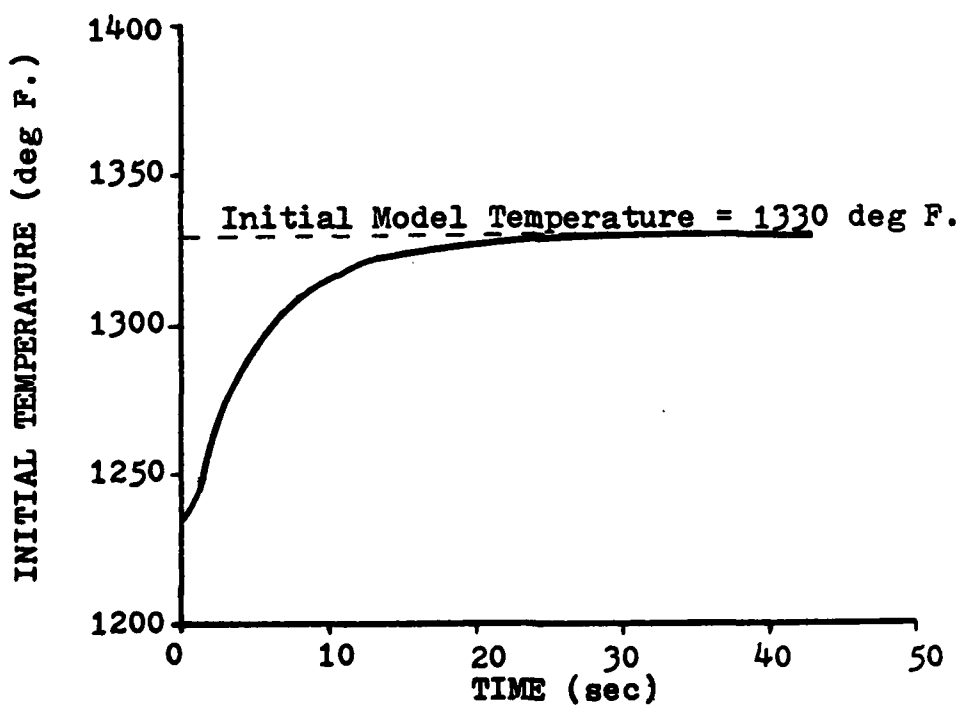


Figure E.3. Initial Condition Smoothing for a Non-Thermocouple Node Point (Node 3)

APPENDIX F

Initial Condition Estimation Flight Data Results

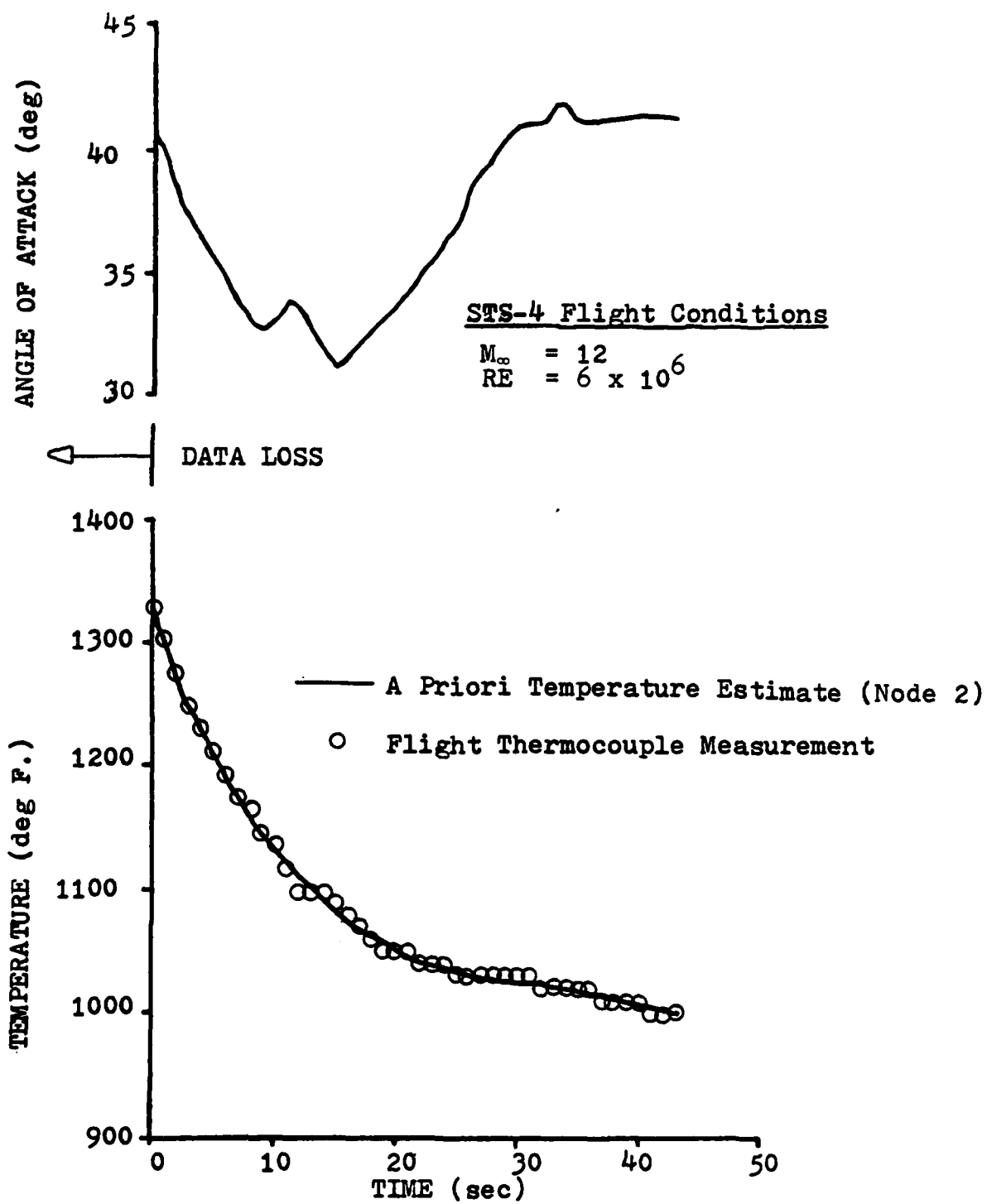


Figure F.1. STS-4 Lower Surface Thermocouple Data with Initial Condition Smoothing (Mach 12 POPU)

TABLE F-1 STS-4 Lower Surface Initial Condition Smoothing

A. Smoothed Initial Temperature

<u>Node</u>	<u>Smoothed Initial Temp. (deg. F.)</u>
1	1330
*2	1330
3	1347
4	1173
*5	1006
6	842
7	781
*8	721
9	626
10	550
*11	430
12	126
13	122

\* Thermocouple Node

B. Parameter Estimates ( $\alpha_0 = 40$  deg. ; Average Error = .03136)

<u>Parameter</u>	<u>Estimate</u>
$\Delta x_A$	.00137 ( $\pm .00016$ )
$q_0$	.06259 ( $\pm .0015$ )
$q_{\alpha_1}$	.00106 ( $\pm .00029$ )

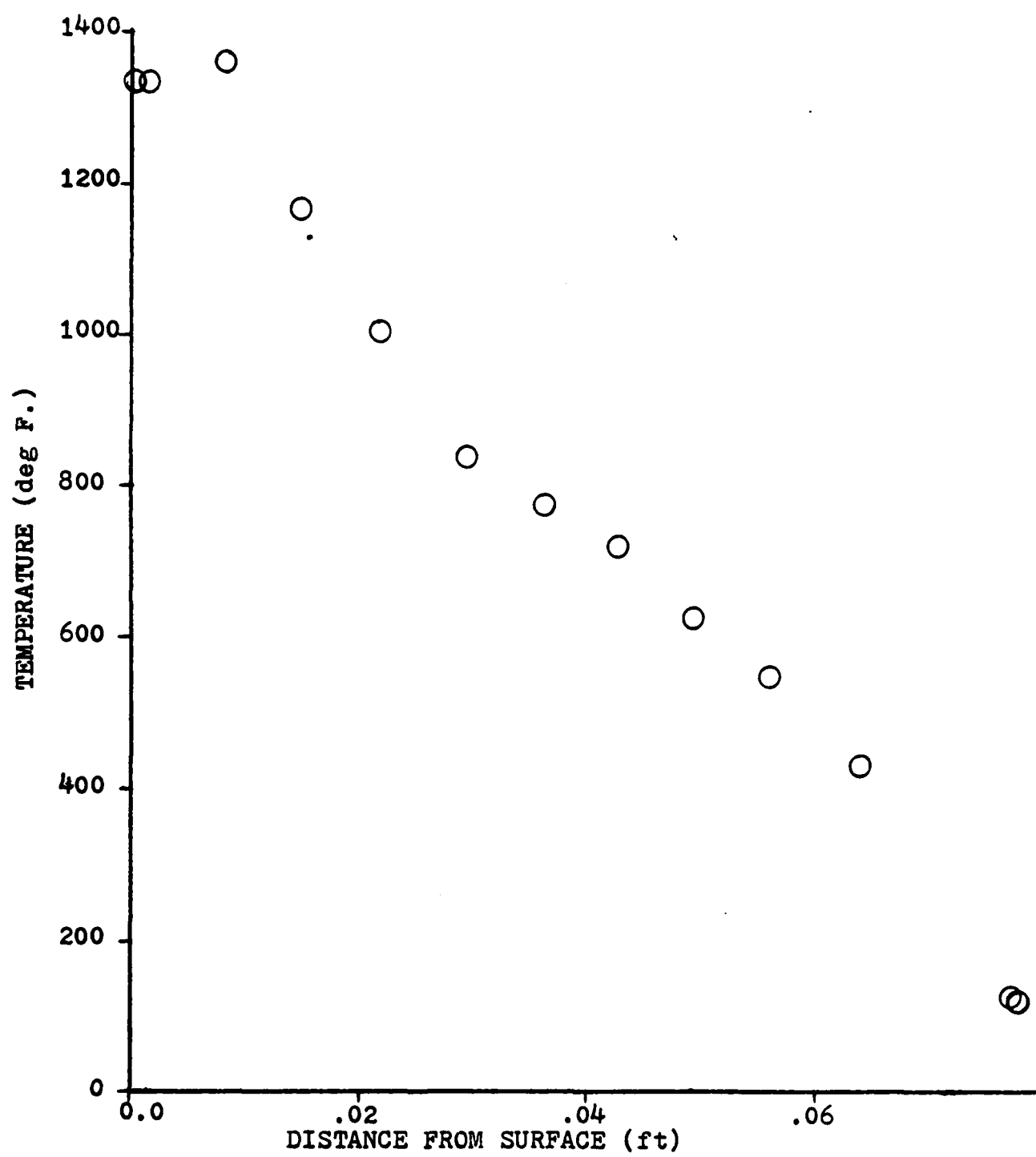


Figure F.2. Smoothed Initial Temperature Profile for STS-4 Lower Surface Plug

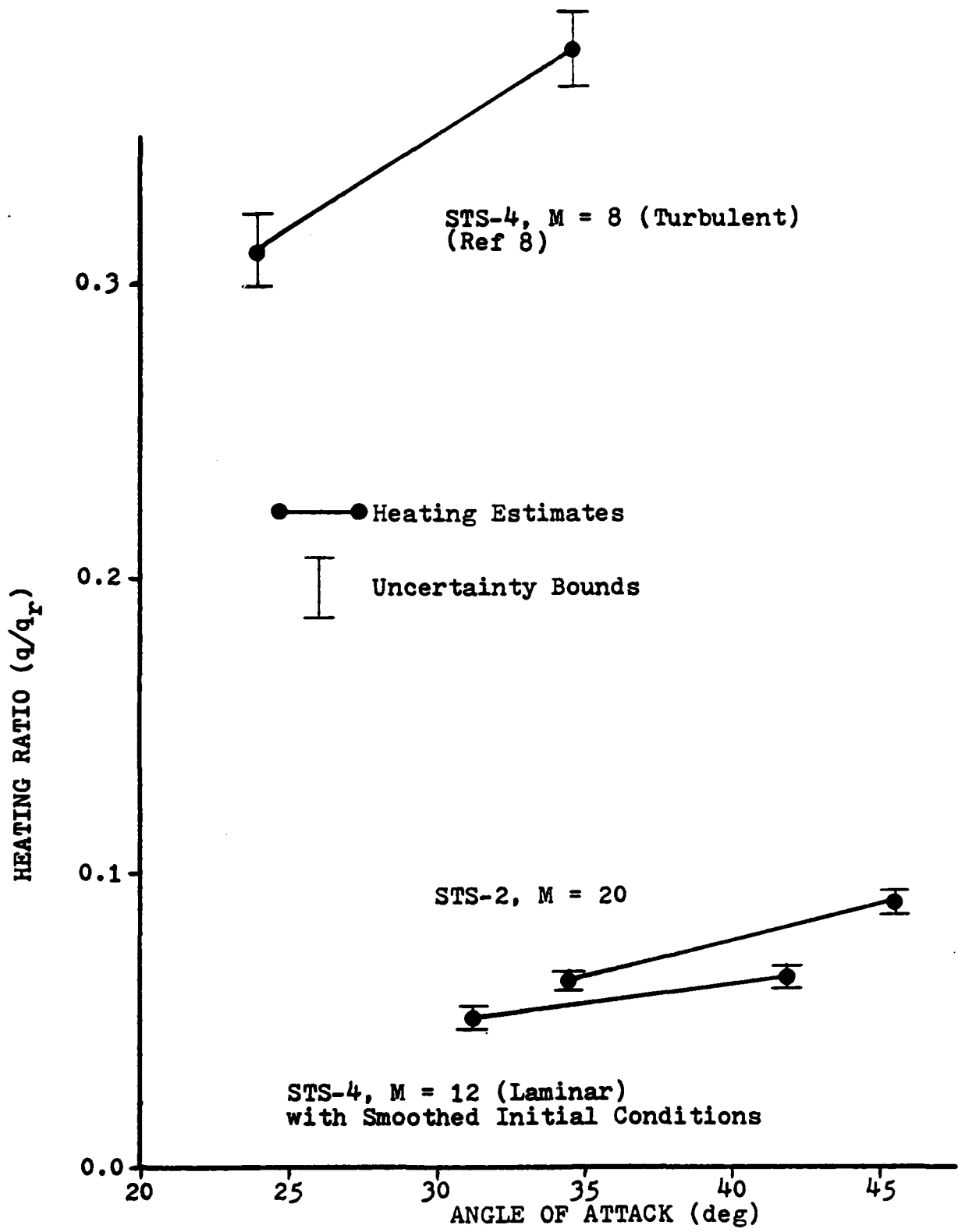


Figure F.3. Heating Estimates for STS-2/STS-4 Lower Surface

Vita

Charles Dyches Lutes was born on 29 October 1960 in New York City, the son of Charles L. and Marilyn D. Lutes. He was raised in Louisville, Kentucky where he graduated from Trinity High School in 1978. He attended Duke University in Durham, North Carolina on an Air Force ROTC scholarship and graduated magna cum laude in May 1982, with a Bachelor's Degree in Mechanical Engineering and Materials Science. Upon his commission in the Air Force, Lt Lutes entered the Air Force Institute of Technology in June of 1982. He is a member of Phi Beta Kappa, Tau Beta Pi, and Pi Tau Sigma.

Permanent Address: 101 Fairway Lane, Route 2  
Barnwell, S. Carolina 29812

**UNCLASSIFIED**

SECURITY CLASSIFICATION OF THIS PAGE

**REPORT DOCUMENTATION PAGE**

1a. REPORT SECURITY CLASSIFICATION <b>UNCLASSIFIED</b>		1b. RESTRICTIVE MARKINGS	
2a. SECURITY CLASSIFICATION AUTHORITY		3. DISTRIBUTION/AVAILABILITY OF REPORT Approved for public release; distribution unlimited	
2b. DECLASSIFICATION/DOWNGRADING SCHEDULE			
4. PERFORMING ORGANIZATION REPORT NUMBER(S) <b>AFIT/GAE/AA/83D-14</b>		5. MONITORING ORGANIZATION REPORT NUMBER(S)	
6a. NAME OF PERFORMING ORGANIZATION <b>School of Engineering</b>	6b. OFFICE SYMBOL <i>(If applicable)</i> <b>AFIT/ENY</b>	7a. NAME OF MONITORING ORGANIZATION	
6c. ADDRESS (City, State and ZIP Code) <b>Air Force Institute of Technology Wright-Patterson AFB, OH 45433</b>		7b. ADDRESS (City, State and ZIP Code)	
8a. NAME OF FUNDING/SPONSORING ORGANIZATION <b>6520 Test Wing</b>	8b. OFFICE SYMBOL <i>(If applicable)</i> <b>TEG</b>	9. PROCUREMENT INSTRUMENT IDENTIFICATION NUMBER	
8c. ADDRESS (City, State and ZIP Code) <b>Edwards AFB, California 93523</b>		10. SOURCE OF FUNDING NOS.	
11. TITLE (Include Security Classification) <b>See Box 19</b>		PROGRAM ELEMENT NO.	PROJECT NO.
12. PERSONAL AUTHORIS. <b>Charles D. Lutes, B.S.E., 2d Lt, USAF</b>		TASK NO.	WORK UNIT NO.
13a. TYPE OF REPORT <b>MS Thesis</b>	13b. TIME COVERED FROM _____ TO _____	14. DATE OF REPORT (Yr., Mo., Day) <b>1983 December</b>	
16. SUPPLEMENTARY NOTATION		17. APPROVED FOR PUBLIC RELEASE: AFIT/AIA/180-17 <i>Lynn E. WOLANSKI</i> Dean for Research and Professional Development	
17. COSATI CODES		18. SUBJECT TERMS (Identify by block number) <b>Space Shuttle; System Identification; Parameter Estimation; Fixed-Point Smoothing; Aerodynamic Heating; Aerothermodynamics</b>	
19. ABSTRACT (Continue on reverse if necessary and identify by block number)  <b>Title: NONLINEAR MODELING AND INITIAL CONDITION ESTIMATION FOR IDENTIFYING THE REENTRY AEROTHERMODYNAMIC ENVIRONMENT OF THE SPACE SHUTTLE ORBITER</b>			
20. DISTRIBUTION/AVAILABILITY OF ABSTRACT <b>UNCLASSIFIED/UNLIMITED <input checked="" type="checkbox"/> SAME AS RPT. <input type="checkbox"/> DTIC USERS <input type="checkbox"/></b>		21. ABSTRACT SECURITY CLASSIFICATION <b>UNCLASSIFIED</b>	
22a. NAME OF RESPONSIBLE INDIVIDUAL <b>James K. Hodge, Captain, USAF</b>		22b. TELEPHONE NUMBER <i>(Include Area Code)</i> <b>(513)-255-3517</b>	22c. OFFICE SYMBOL <b>AF /ENY</b>

**UNCLASSIFIED**

**SECURITY CLASSIFICATION OF THIS PAGE**

This report describes improvements made to the data analysis tool HEATEST, used for identification of the reentry aerothermodynamic environment of the Space Shuttle Orbiter. The heating model was changed from a linear perturbation form to that of a piecewise linear interpolation form to account for nonlinear heating rates. Also, a fixed-point initial condition smoother was incorporated to gain better estimates of unknown initial temperatures. The development of both of these improvements is described, as well as the overall adaptive estimation process employed by the HEATEST scheme. Verification of these modifications was accomplished by applications to both simulated and actual flight test data.

Simulations of nonlinear heating rates indicated higher than actual coating thickness predictions for the linear perturbation model previously used. Flight results using the improved heating model provided additional verification of a time skew due to nonisothermal wall effects on the OMS pod. Initial condition smoothing enabled the identification of an unmodelled Mach or Reynolds number effect on the lower surface during the Mach 12 Pushover Pullup maneuver of STS-4.

**UNCLASSIFIED**

**SECURITY CLASSIFICATION OF THIS PAGE**

END

FILMED

2-84

DTIC